CHAPTER–6

Unravelling the Potential of Tripodal Vanadium Catalysts for Dinitrogen Reduction

Abstract: Density functional theory calculations have been carried out to screen the potential of several tripodal vanadium complexes towards conversion of dinitrogen to ammonia as a function of different equatorial (P^iPr_2 and S^iPr) and bridgehead groups (B, C and Si). The proposed complexes were probed towards understanding their efficiency in some of the key steps involved in the dinitrogen fixation process. All the complexes were found to be successful in preventing the release of hydrazine during the nitrogen reduction reaction. We have performed a comprehensive mechanistic study by considering all the possible pathways (distal, alternate and hybrid) to understand the efficiency of some of the proposed catalysts towards dinitrogen reduction process. The exergonic reaction free energies obtained for some of the key steps as well as the presence of thermally surmountable barrier heights involved in the catalytic cycle indicate that the proposed vanadium complexes may be considered as suitable platforms for the functionalization of dinitrogen.

[6.1] Introduction

The element nitrogen is essential for life on earth. Although dinitrogen is one of the most available molecules surrounding us, its high thermodynamic stability (945 kJ mol^{-1}) [1] and nonpolar nature makes it inert, and hence difficult to use in different chemical processes. Industrially, the best method known to date for the reduction of dinitrogen to ammonia is the Haber-Bosch process, which demands a high temperatures (400–500 °C) and pressures (~200 atm) [2-3]. Interestingly, the same process is performed by nature under ambient conditions with the assistance of a group of enzymes known as nitrogenases, which contain transition metals (TM) such as Fe (iron-only nitrogenase), Mo (molybdenum nitrogenase) and V (vanadium nitrogenase) in their active sites [4]. The enzyme nitrogenase contains two protein units - the larger one (Fe-Mo protein) consists of two P-clusters, which help in the electron transfer process, while the other unit contains two iron-molybdenum cofactors (FeMocos) where reduction of dinitrogen takes place [5-6]. Therefore, efforts are being made to mimic the active sites of nitrogenase enzymes by developing suitable TM-based model systems that can carry out the reduction process under ambient conditions [7-10].

In 2003, Schrock and coworkers synthesized the first nitrogenase model system that can catalytically convert dinitrogen into ammonia [11] using a molybdenum complex (**I**, Scheme 6.1) that contain the sterically encumbered $[HIPTN_3N]^{3-}$ ligand, where HIPT = 3,5-(2,4,6-$^{i}Pr_3C_6H_2)_2C_6H_3$ (hexaisopropylterphenyl). Lutidinium [Lut] and decamethylchromocene were used as proton source and reductant, respectively, and the overall yield was found to be 66%. In order to understand the mechanistic details of the N_2 reduction process, several intermediates were isolated and DFT calculations were performed [12-19]. A few years later, in 2011, Nishibayashi and coworkers developed a dinuclear molybdenum dinitrogen complex (**III**) supported by a PNP pincer ligand that can produce up to 11.6 equivalents of NH_3 per molybdenum center by employing cobaltocene as reductant and lutidinium triflate as proton source [20]. Following this, they have reported a number of molybdenum-based pincer-type catalysts that can effectively convert dinitrogen to ammonia under mild reaction conditions [9-10]. Furthermore, in 2017, the same group developed another dinuclear molybdenum system with *N*-heterocyclic carbene (NHC)-based PCP pincer ligands (**IV**) that shows remarkable catalytic activity towards the reduction of dinitrogen to ammonia (230 equiv. of NH_3) − the most effective catalyst synthesized to date [21]. The introduction of the

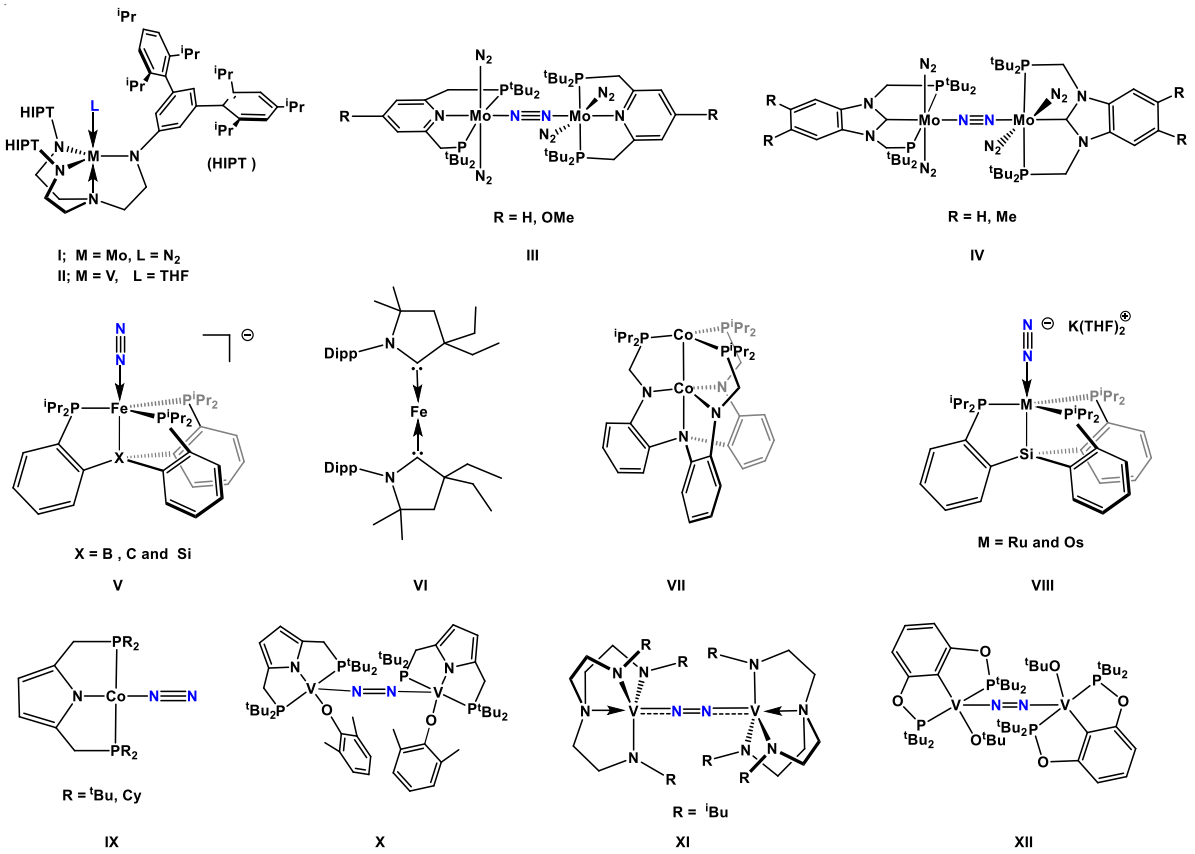

Scheme 6.1: Schematic representation of some synthetically amenable catalysts for nitrogen fixation.

carbene moiety into the PCP pincer ligand makes it not only a good σ donor but also a good π acceptor, which results in stronger interaction between the molybdenum center and the pincer ligand. Thus, the system can stabilize different reaction intermediates throughout the course of reaction.

Over the years, Peters and coworkers have synthesized and characterized a number of iron-based model systems (**V**) that can mimic the biological activity of nitrogenase enzyme [22-25]. Out of these model systems that have boron, carbon and silicon as the bridgehead atoms, the best results were obtained for the boron anchored example, which may be attributed to the flexibility of the Fe····B bond. The presence of a flexible Fe····B linkage allows the system to stabilize different intermediates (where Fe exists in various oxidation states) formed during the course of the reduction process, and results in better yields of ammonia (64 equiv. of NH_3) [26]. The same group also synthesized a dicoordinate iron complex containing two CAAC (cyclic

alkyl(amino)carbene) ligands which can not only bind dinitrogen but can also reduce it to ammonia (4.7 equiv. NH_3) at low temperature (**VI**) [27].

Most of the model systems that have been designed to date contain iron or molybdenum as the central atom. However, a number of model systems with transition metals other than iron and molybdenum have also been reported [28]. For example, Lu and coworkers have synthesized a dicobalt complex (**VII**) which could mediate the catalytic conversion of dinitrogen to silylamines under ambient conditions [29]. On the other hand, Peters and coworkers successfully synthesized tris(phosphine)silyl-ligand-supported osmium and ruthenium complexes (**VIII**) that are capable of converting dinitrogen to ammonia under ambient pressure and at low temperatures [30]. Similarly, in 2016, Nishibayashi and coworkers reported the binding of dinitrogen to a cobalt PNP pincer complex (**IX**) [31]. In 2006, Schrock and coworkers successfully synthesized the vanadium analog of **I** (**II**) [32], which, however, failed to produce ammonia under similar reaction conditions. We performed a detailed computational study to understand the reasons behind the poor performance of **II** towards conversion of N_2 to NH_3 [33]. In a ground-breaking study, Nishibayashi and coworkers reported the synthesis and isolation of the first vanadium-based catalyst (**X**) that could catalytically convert N_2 to NH_3 under mild reaction conditions [34]. Kajita and coworkers synthesized a couple of dinitrogen-divanadium complexes (**XI**) supported by triamidoamine ligands, which, upon reaction with proton source (HOTf, HCl and [Lut]OTf) and reductant ($M[C_{10}H_8]$, M = Na, K), led to the direct reduction of N_2 to NH_3 without generating hydrazine [35-36]. Very recently, Hu and coworkers reported the synthesis of a divanadium pincer complex (**XII**) that can catalytically convert N_2 to NH_3 and N_2H_4 [37]. It is pertinent to mention here that in terms of efficiency, the vanadium nitrogenase stands next to the molybdenum nitrogenase. However, only a limited number of vanadium-based complexes are known that can catalytically facilitate the conversion of dinitrogen to ammonia [38]. Therefore, there is not only ample scope but also a need to design and study a variety of biomimetic vanadium-based systems for the nitrogen reduction reaction (NRR). Herein, we present the results of a comprehensive computational study on the potential of several tripodal vanadium complexes (Scheme 6.2) in the conversion of N_2 to NH_3, with special emphasis on some of the key steps involved in NRR such as protonation of the metal-dinitrogen complex and formation of the metal nitride

complexes etc. Furthermore, we have compared the energetics obtained for our proposed vanadium complexes with those of Schrock's vanadium complex (**II**) [39].

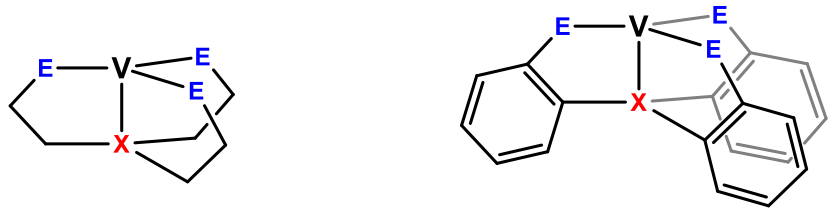

E = P^{i}Pr$_2$, X = C (1a')
X = Si (1b')
X = B (1c')
E = S^{i}Pr, X = C (1d')
X = Si (1e')
X = B (1f')

E = P^{i}Pr$_2$, X = C (1a'')
X = Si (1b'')
X = B (1c'')
E = S^{i}Pr, X = C (1d'')
X = Si (1e'')
X = B (1f'')

Scheme 6.2: Schematic representation of the model vanadium complexes considered in this study.

[6.2] Computational Details:

Density functional theory (DFT) calculations were performed to optimize all the molecules without any symmetry constraints by employing M06-L functional [40] in conjunction with 6-311+G* basis set for all the elements [41-43]. Our choice of the M06-L functional was prompted by previous reports of its suitability in not only reproducing experimental geometries but also in estimating or predicting reaction energies of organometallic systems [44-52]. We had verified this further by reproducing the experimentally observed geometrical parameters for some synthetically achievable vanadium complexes [32,34] (Figure 6.1). Frequency calculations were performed at the same level of theory to check the nature of the stationary points. All the ground-state structures were characterized by real frequencies while the transition states (TS) were characterized by the presence of only one imaginary frequency. The authenticities of the TSs were further probed by performing intrinsic reaction coordinate calculations (IRC) at the same level of theory. The polarized continuum model (PCM) was employed to include solvation effects for the solution-phase calculations using heptane as the solvent [53]. Free energies corresponding to the protonation and reduction steps were evaluated relative to the processes $LutH^+ \rightarrow Lut + H^+$ and $[Cp^*_2Cr] \rightarrow [Cp^*_2Cr]^+ + e^-$, respectively, without any structural modification of the molecules involved (Cp^*_2Cr =

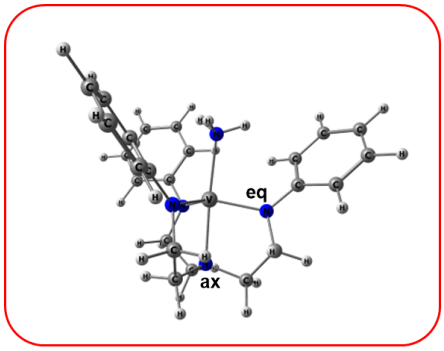

Geometrical parameters	Calculated values	Experimental values	difference
$V–N_{eq}$	1.955	1.972	0.017
$V–N_{eq}$	1.957	1.989	0.032
$V–N_{eq}$	1.952	1.975	0.023
$V–N_{ax}$	2.148	2.200	0.052
$V–NH_3$	2.162	2.215	0.053

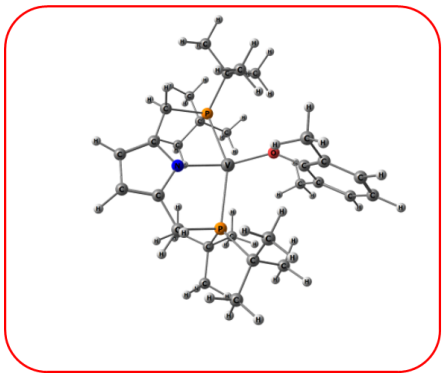

Geometrical parameters	Calculated values	Experimental value	difference
V–N	2.055	2.038	0.017
V–P	2.561	2.587	0.026
V–P	2.529	2.538	0.009
V–O	1.926	1.905	0.021

Figure 6.1: Comparison of the available X-ray data and our calculated (M06-L-D3(heptane)/6-311+G*) values of the important geometrical parameters for the experimentally known vanadium complexes [32,34]. Bond lengths are given in Å.

decamethyl chromocene and Lut = 2,6-dimethylpyridine). Dispersion effects were incorporated by using the D3 version of Grimme's dispersion correction coupled with the original D3 damping function with the keyword Empiricaldispersion=GD3 [54]. The ultrafine grid was used throughout the calculations. Natural bonding orbital analysis was performed using the natural bond orbital (NBO) [55] scheme as implemented in the Gaussian 09 suite of programs [56]. In order to determine the activation energy barrier between species that have different ground-state multiplicities (spin states), the probable TSs were searched in all possible spin states, and the barrier height was computed by considering the lowest energy TS [57,58]. Furthermore, since all the nitrogenous species involved in the catalytic cycle can exhibit more than one multiplicity, optimization of each species was performed by considering all the possible spin states, and the reaction free energies were calculated by considering the lowest-energy spin state. The energetics for all the calculations were evaluated in terms of changes in Gibbs free energies at 1 atm pressure and 298 K temperature, unless otherwise specified.

[6.3] Results and discussion

Before proceeding to study the entire NRR catalytic cycle, we decided to investigate the efficiency of the proposed catalysts in performing some key steps of the NRR as detailed below.

[6.3.1] Formation of the diazenido complex

The optimized structures of the starting complexes **[1a′]–[1f′]** and **[1a″]–[1f″]** (Scheme 6.2) possess a trigonal monopyramidal geometry with the pyramidalization angle ($\theta = 360 - \Sigma\angle$E–V–E, E = S and P) at the vanadium center varying from 1.8–11.0° (Figure 6.2 and Table 6.1). Further, complexes with carbon or silicon as the bridgehead atoms may give rise to three different spin states viz., singlet, triplet and quintet with the quintet states being the most stable (the singlet and triplet states lie higher in energy by 13-33 kcal mol^{-1} and 5-26 kcal mol^{-1} respectively). Accordingly, we have considered only the quintet state geometry for the complexes with carbon and silicon as bridgehead groups in our study. Similarly, three different spin states, viz., doublet,

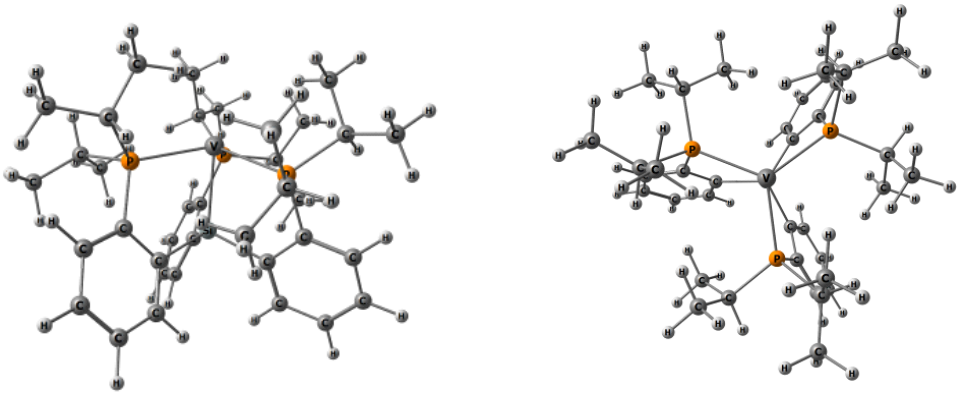

Figure 6.2: Optimized geometry of a representative vanadium complex (E = P^iPr_2 and X = Si) in two different orientations: (a) side view and (b) top view.

quartet and sextet may be envisioned for vanadium complexes with boron as the bridgehead atom, and calculation of the relative energies of the spin state for **[1c′]** reveals that the sextet state is the most stable one (the quartet and doublet states lie higher in energy by 11.4 and 23.4 kcal mol^{-1} respectively). However, for **[1f′]**, the sextet and quartet states are isoenergetic (the energy difference between these states is only 1.3 kcal mol^{-1}), therefore, we have considered the sextet geometry for further study. However, the unsaturated vanadium complexes **[1c″]** and **[1f″]** computes the quartet

state as their ground state with a distorted geometry. Therefore, their sextet state geometries were considered for further discussion. The important geometrical parameters of the vanadium complexes in their ground state are listed in Table 6.1.

Table 6.1: Calculated (M06-L-D3(heptane)/6-311+G*) important geometrical parameters, natural charges and pyramidalization angle (in degree) at the metal (θ_V) and apical (θ_X, X = B, C and Si) center for the Schrock catalyst (**II**) and model vanadium complexes considered in this study. Also, given are the energies (in eV) of the donor (E_{HOMO}), acceptor (E_{LUMO}) orbitals (centered at the transition metal center) of the parent vanadium complexes **[1a′]-[1f′]**, **[1a″]-[1f″]** and **II**. Bond lengths are given in Å and WBI values are given within parenthesis.

Molecules	**V-E**	**V-X**	$\mathbf{q_V}$	$\mathbf{q_X}$	$\boldsymbol{\theta_V/\theta_X}$	$\mathbf{E_{HOMO}}$	$\mathbf{E_{LUMO}}$
II	1.955	2.113	1.179	-0.567	3.7/20.7	-4.09	-1.90
	(0.662)	(0.350)					
[1a′]	2.484	2.259	-0.094	-0.384	3.9/35.2	-2.41	-1.12
	(0.501)	(0.556)					
[1b′]	2.494	2.489	-0.375	1.142	8.1/34.6	-2.47	-1.39
	(0.509)	(0.792)					
[1c′]	2.464	2.664	-0.139	0.726	6.7/10.7	-2.56	-1.37
	(0.445)	(0.233)					
[1d′]	2.491	2.201	0.042	-0.403	1.9/31.0	-2.02	-0.91
	(0.472)	(0.571)					
[1e′]	2.492	2.465	-0.260	1.129	6.2/30.5	-2.32	-1.04
	(0.493)	(0.849)					
[1f′]	2.484	2.496	0.024	0.640	2.5/9.6	-2.16	-1.10
	(0.437)	(0.260)					
[1a″]	2.473	2.259	0.044	-0.404	8.0/24.1	-2.69	-1.38
	(0.484)	(0.435)					
[1b″]	2.477	2.432	-0.383	1.166	11.0/34.0	-2.78	-1.41
	(0.492)	(0.742)					
[1c″]	2.486	2.490	-0.027	0.614	6.6/13.7	-2.84	-1.49
	(0.447)	(0.225)					
[1d″]	2.456	2.185	0.168	-0.432	1.8/26.7	-2.58	-1.39
	(0.497)	(0.514)					
[1e″]	2.510	2.392	-0.120	1.102	5.9/32.6	-2.51	-1.38
	(0.452)	(0.843)					
[1f″]	2.463	2.409	0.156	0.541	2.3/13.4	-2.68	-1.29
	(0.449)	(0.252)					

Three different pathways, viz., **A**, **B** and **C** may be envisioned for the conversion of the bare complex (**[1]**) to the diazenido complex (**[4]**) as shown in Figure 6.3. However, earlier computational studies have suggested pathway **B** to be the most viable route for converting the parent complex into the neutral diazenido complex [16, 33, 59]. Accordingly, we have considered the pathway **B** to investigate the potential of our proposed vanadium complexes towards formation of the diazenido complex. The first step for pathway **B** involves binding of N_2 to the bare complex **[1]** yielding **[2]** (**[V]-N_2**). Complex **[2]** with either carbon or silicon as the bridgehead atom can exhibit three different spin states (singlet, triplet and quintet) with the quintet state being the most stable . Hence, their quintet states were considered for further study.

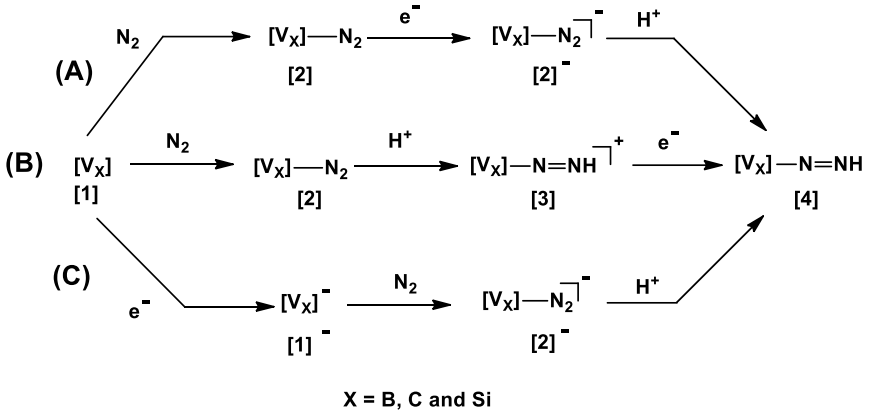

Figure 6.3: The three possible pathways **A**, **B** and **C** for the conversion of **[1]→[4]**.

However, vanadium dinitrogen complexes with boron as the bridgehead atom (**[2c′]**, **[2c′′]**, **[2f′]** and **[2f′′]**) computes the sextet state as their ground state. Further, it is to be noted that all the vanadium dinitrogen complexes exhibit a trigonal bipyramidal geometry (TBP) with the pyramidalization angle around the TM center ranging from 4.6–20.0° (Table 6.2). Furthermore, MO analysis of **[1a′]**–**[1f′]**, **[1a′′]**–**[1f′′]** and **II** reveals that all the bare vanadium complexes considered in this study exhibit substantially higher Lewis basicity (E_{HOMO} = -2.0 to -2.8 eV, Table 6.1) compared to that of **II** (E_{HOMO} = -4.1 eV). In addition, the calculated natural charges at the TM center are found to be relatively more negative in **[1a′]-[1f′]** (0.024 to -0.375) and **[1a′′]**–**[1f′′]** (0.044 to -0.383) compared to that in **II** (1.179) further corroborating the higher Lewis basicity of our proposed complexes (Table 6.1). Therefore, in all the dinitrogen adducts of **[1a′]-[1f′]** and **[1a′′]**–**[1f′′]**, a higher degree of backdonation from the filled metal

orbitals to the antibonding molecular orbitals of dinitrogen ($V\rightarrow\pi^*_{N\equiv N}$) can be expected. Indeed, the reaction **[1a′]→[2a′]** (Table 6.3), i.e. the binding of N_2 with

Table 6.2: Calculated (M06-L-D3(heptane)/6-311+G*) important geometrical parameters and natural charge at the metal (V) and α (q_{N_α}) and β (q_{N_β}) nitrogen atoms of the dinitrogen complexes of Schrock catalyst and model vanadium complexes considered in this study. Bond lengths are given in Å and WBI values are given within parenthesis.

Molecule	V-E	V-X	V-N	N≡N	ν(N≡N)	q_V	q_{N_α}	q_{N_β}	θ_M/θ_X
II-N_2	1.960	2.182	2.081	1.114	2229.66	0.887	-0.008	0.086	5.9/22.8
	(0.774)	(0.360)	(0.598)	(2.773)					
[2a′]	2.492	2.332	2.019	1.135	2029.86	-0.394	-0.099	-0.061	8.1/36.9
	(0.602)	(0.543)	(0.697)	(2.529)					
[2b′]	2.509	2.563	2.006	1.139	2003.09	-0.811	-0.118	-0.070	13.8/36.8
	(0.628)	(0.772)	(0.712)	(2.499)					
[2c′]	2.488	2.967	2.001	1.138	2009.86	-0.285	-0.180	-0.059	20.0/9.3
	(0.510)	(0.164)	(0.623)	(2.491)					
[2d′]	2.519	2.262	2.016	1.136	2025.25	-0.159	-0.127	-0.066	4.9/33.6
	(0.542)	(0.544)	(0.712)	(2.511)					
[2e′]	2.534	2.543	2.010	1.139	2004.15	-0.523	-0.138	-0.073	11.4/32.2
	(0.546)	(0.833)	(0.733)	(2.495)					
[2f′]	2.501	2.658	2.008	1.136	2027.92	-0.159	-0.153	-0.057	9.1/11.0
	(0.508)	(0.226)	(0.670)	(2.512)					
[2a″]	2.491	2.331	2.013	1.134	2037.3	-0.261	-0.104	-0.044	13.0/26.0
	(0.581)	(0.420)	(0.683)	(2.537)					
[2b″]	2.537	2.503	2.023	1.133	2043.4	-0.679	-0.115	-0.044	15.9/38.0
	(0.576)	(0.726)	(0.641)	(2.549)					
[2c″]	2.521	2.612	2.009	1.134	2041.6	-0.220	-0.142	-0.037	13.7/15.5
	(0.507)	(0.194)	(0.619)	(2.535)					
[2d″]	2.476	2.251	2.023	1.132	2058.4	-0.119	-0.100	-0.039	4.6/29.3
	(0.577)	(0.488)	(0.712)	(2.559)					
[2e″]	2.523	2.473	2.021	1.135	2033.7	-0.507	-0.124	-0.051	10.1/35.3
	(0.554)	(0.840)	(0.714)	(2.534)					
[2f″]	2.480	2.532	2.015	1.132	2060.7	-0.111	-0.125	-0.029	7.0/15.8
	(0.528)	(0.237)	(0.670)	(2.558)					

[1a′] is found to be appreciably exergonic by -21.1 kcal mol^{-1}, whereas **II** computes only a slightly exergonic (-1.2 kcal mol^{-1}) reaction free energy for the formation of **II-N_2** (Table 6.3). In addition, akin to **[1a′]**, all the newly proposed vanadium complexes (**[1b′]-[1f′]** and **[1a″]**–**[1f″]**) compute substantially exergonic reaction free energies (-18.0 to -23.0 kcal mol^{-1}, Table 6.3) for the formation of the dinitrogen adduct, thereby indicating their potential in N_2 binding. Also, we observed a substantial lowering of vibrational stretching frequency of N_2 in all the N_2 adducts of **[1a′]-[1f′]** and **[1a″]**–**[1f″]** (ν_{NN} = 2003.1–2060.7 cm^{-1}, Table 6.2) compared to that in the free dinitrogen (2412.3 cm^{-1}, calculated at the same level of theory) and **II-N_2** complex (2229.6 cm^{-1}).

Table 6.3: Calculated (M06-L-D3(heptane)/6-311+G*) reaction free energies (in kcal mol^{-1}) for different steps involved in the formation of the diazenido complex (**4**) from the bare complex (**1**) via pathway **B** for the catalysts **[1b′]-[1f′]**, **[1a″]**–**[1f″]** and **II**.

Molecules	1→2	2→3	3→4	Molecules	1→2	2→3	3→4
a′	-21.1	-6.0	-1.8	**a″**	-20.4	0.7	-5.8
b′	-23.0	-3.9	-7.9	**b″**	-18.0	3.2	-7.8
c′	-23.0	-0.7	-4.4	**c″**	-19.1	5.5	-12.2
d′	-22.1	0.4	-5.4	**d″**	-18.7	6.7	-9.2
e′	-22.3	-1.6	-4.0	**e″**	-22.0	8.3	-12.9
f′	-22.2	0.2	-4.2	**f″**	-19.1	8.7	-11.1
II	-1.2	38.4	-38.1				

Furthermore, it is to be noted that the metal−nitrogen (N_α) bonds (V–N_α) in the saturated [V]-N_2 complexes were found to be somewhat stronger than that in the corresponding unsaturated analogs (Table 6.2). For example, the calculated V–N_α bond in **[2b′]** (WBI = 0.712) was computed to be relatively stronger than that in the unsaturated analog **[2b″]** (WBI = 0.641). Such strengthening of the V–N_α bonds in the saturated dinitrogen complexes may be attributed to the relatively high Lewis basicity of **[1a′]-[1f′]** (Table 6.1), which in turn facilitates enhanced backdonation from the metal center to the $\pi^*_{N\equiv N}$ orbital. This is also reflected in the significant lowering of the N≡N stretching frequency

in the saturated dinitrogen complexes (**[2a′]-[2f′]**) compared to that in their unsaturated analogs (**[2a′′]-[2f′′]**) (Table 6.2). In addition, **[1a′]-[1f′]** compute relatively more exergonic reaction free energies for the binding of dinitrogen compared to **[1a′′]-[1f′′]** (Table 6.3).

The second step in pathway **B**, namely protonation of **[2]** to generate **[3]**, is either marginally exergonic or endergonic in nature (-6.0 to 8.7 kcal mol^{-1}). The final step is the reduction of complex **[3]**, thereby affording a neutral diazenido complex **[4]** (**[V]-N=NH**). The reaction free energies associated with this reduction step for the catalysts **[1a′]-[1f′]** and **[1a′′]–[1f′′]** are computed to be exergonic in nature (–1.8 to –12.9 kcal mol^{-1}). Therefore, all the steps involved in pathway **B** for our proposed vanadium complexes are thermodynamically favorable, indicating their potential to form the diazenido complex.

One of the important steps in N_2 reduction chemistry is the initial protonation of the dinitrogen molecule that results in elongation of the N–N bond. For vanadium complexes with P^iPr_2 as the equatorial group (**[2a′]–[2c′]** and **[2a′′]–[2c′′]**), protonation may occur either directly at the distal nitrogen atom (N_β) or at the vanadium atom as shown in Figure 6.4 for complex **[2a′]** as a representative example. The former takes place in the second step of pathway **B** forming the complex **[3a′]**. Furthermore, for the nitrogenous species **[3]** with carbon and silicon as the bridgehead group, two spin states are possible (singlet and triplet) with the triplet state being more stable than the singlet ones by 7.0–18.8 kcal mol^{-1} . Similarly, for complex **[3]** with boron as the bridgehead

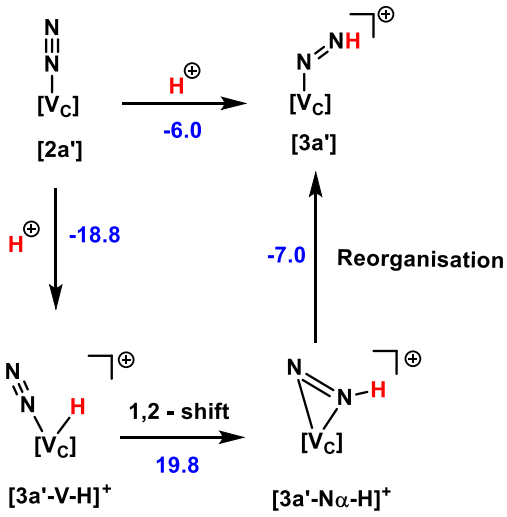

Figure 6.4: Different possibilities for protonation of **[2a′]**. Free energy values are in kcal mol^{-1} calculated at M06-L-D3(heptane)/6-311+G* level of theory.

group, two different spin states were considered viz., doublet and quartet, with the latter being more stable . However, for [V]-N_2 complexes with S^iPr as an equatorial group (**[2d′]–[2f′]** and **[2d′′]–[2f′′]**), protonation may take place not only at the TM center and N_β, but also at the equatorial sulfur atom. Therefore, in the present study, we have considered all three possibilities for **[2d′]–[2f′]** and **[2d′′]–[2f′′]**. However, the reaction free energies obtained for protonation at the equatorial sulfur atom of **[2d′]–[2f′]** and **[2d′′]–[2f′′]** were substantially endergonic (16.9-22.2 kcal mol^{-1}, Table 6.4) thereby ruling out such a possibility. The endergonicity associated with the protonation at S^iPr may be traced to the higher stability of the lone pair at the sulfur atoms (Figure 6.5).

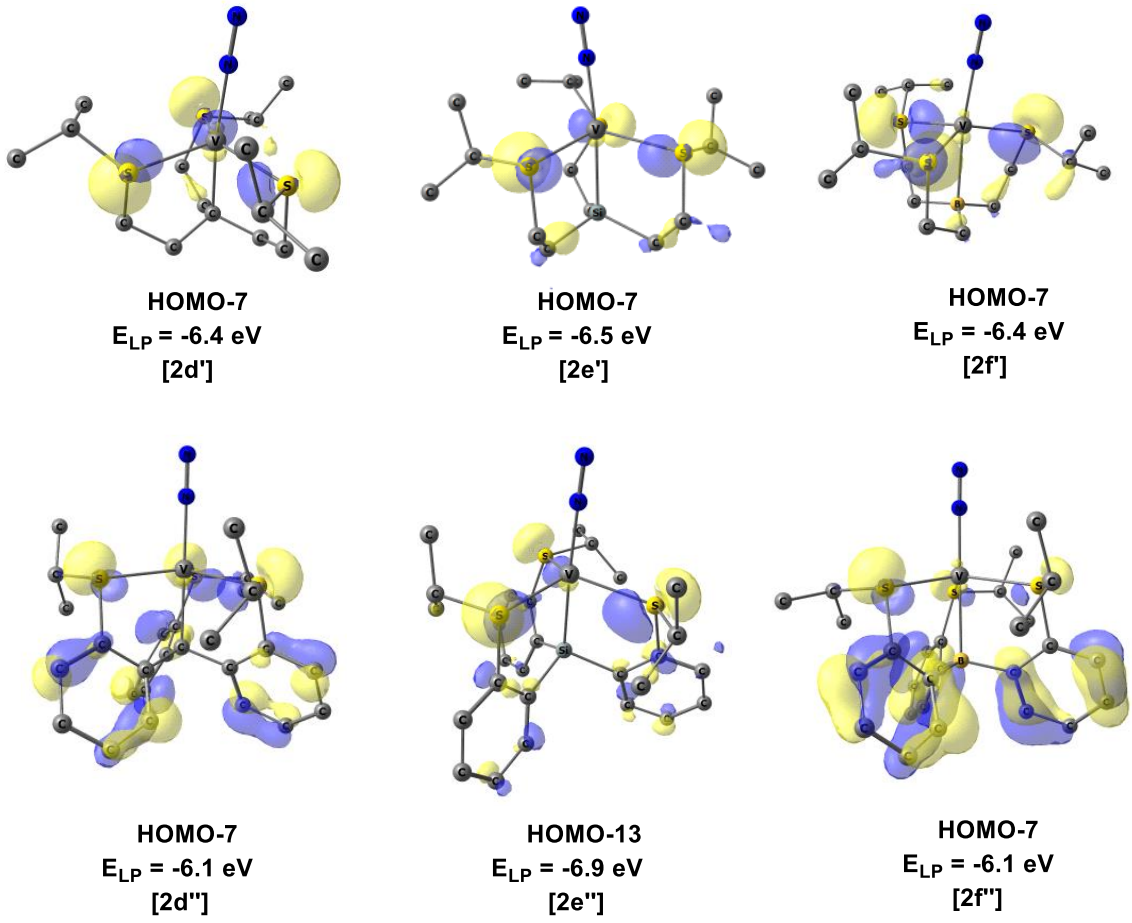

Figure 6.5: Pictorial representation of the molecular orbital showing the lone pairs situated at the sulphur atoms of the dinitrogen vanadium complexes **[2a′]-[2f′]** and **[2a′′]-[2f′′]**.The hydrogen atoms of the methyl groups are omitted for the sake of clarity.

Table 6.4: Calculated reaction free energies for the protonation of the equatorial sulphur and nitrogen atom, metal center and distal nitrogen atom of the dinitrogen complexes **[2a′]-[2f′]** and **[2a″]-[2f″]** and **II**.

Molecules	S/N	V	N_β	Molecules	S/N	V	N_β
II	-7.0	29.7	38.4	**[2a″]**	-	-12.2	0.7
[2a′]	-	-18.8	-6.0	**[2b″]**	-	-13.5	3.2
[2b′]	-	-17.8	-3.9	**[2c″]**	-	-12.2	5.5
[2c′]	-	-21.3	-0.7	**[2d″]**	19.7	-14.5	6.7
[2d′]	19.3	-17.4	0.4	**[2e″]**	16.9	-11.3	8.3
[2e′]	16.9	-19.6	-1.6	**[2f″]**	22.2	-15.2	8.7
[2f′]	19.7	-25.3	0.2				

Furthermore, the metal centers of **[2a′]–[2f′]** and **[2a″]–[2f″]** are highly basic in nature, which is not only evident from the calculated natural charges (Table 6.2) but also from the fact that the HOMO is localized at vanadium (Figure 6.6). In agreement with this observation, direct protonation at the metal center is found to be considerably more exergonic (-18.8 kcal mol^{-1}) than protonation at the distal nitrogen (N_β) atom (-6.0 kcal mol^{-1}) as shown in Figure 6.4. A similar trend is observed for all other vanadium complexes proposed in this study (Table 6.4). However, in order to activate the N–N bond, the proton has to bind to the distal nitrogen atom, thereby generating **[3]**. Accordingly, we have searched for the possible pathway for the conversion of **[3a′-V-H]**$^+$ to **[3]**. As shown in Figure 6.4, the metal-protonated species **[3a′-V-H]**$^+$ first undergoes a 1,2-proton shift to generate the η^2-type intermediate **[3a′-N_α-H]**$^+$, which then undergoes reorganization, generating **[3a′]** in its triplet ground state. The 1,2-shift process was considerably endergonic (19.8 kcal mol^{-1}) while the reorganization of **[3a′-N_α-H]**$^+$ was exergonic by -7.0 kcal mol^{-1}. We have also calculated the activation energy barrier ($\Delta G^{\ddagger}$) associated with the conversion of **[2a′]** to **[3a′]** via the intermediate **[3a′-N_α-H]**$^+$ by locating the probable transition states (Figure 6.7). The activation energy barriers associated with the 1,2-proton shift (+40.7 kcal mol^{-1}) and reorganization process (+16.7 kcal mol^{-1}) are quite high and hence, the metal protonated species **[3a′-V-H]**$^+$ is unlikely to generate **[3a′]** (**[V^{III}]–N=NH**$]^+$). The optimized geometries of the TSs (**TS1** and **TS2**) and intermediate involved in the formation of **[2]**→**[3]** (via metal-

protonated species) for all the vanadium complexes are shown in Figures 6.8-6.10 and the energetics are listed in Table 6.5. Similar to **[2a′]**, the metal-protonated species of **[2b′]–[2f′]** and **[2a′′]–[2f′′]** are not expected to produce complex **[3]** because of the significantly higher barrier heights associated with their conversion (Table 6.5). Therefore, it can be concluded that the most likely pathway for the generation of **[3]**

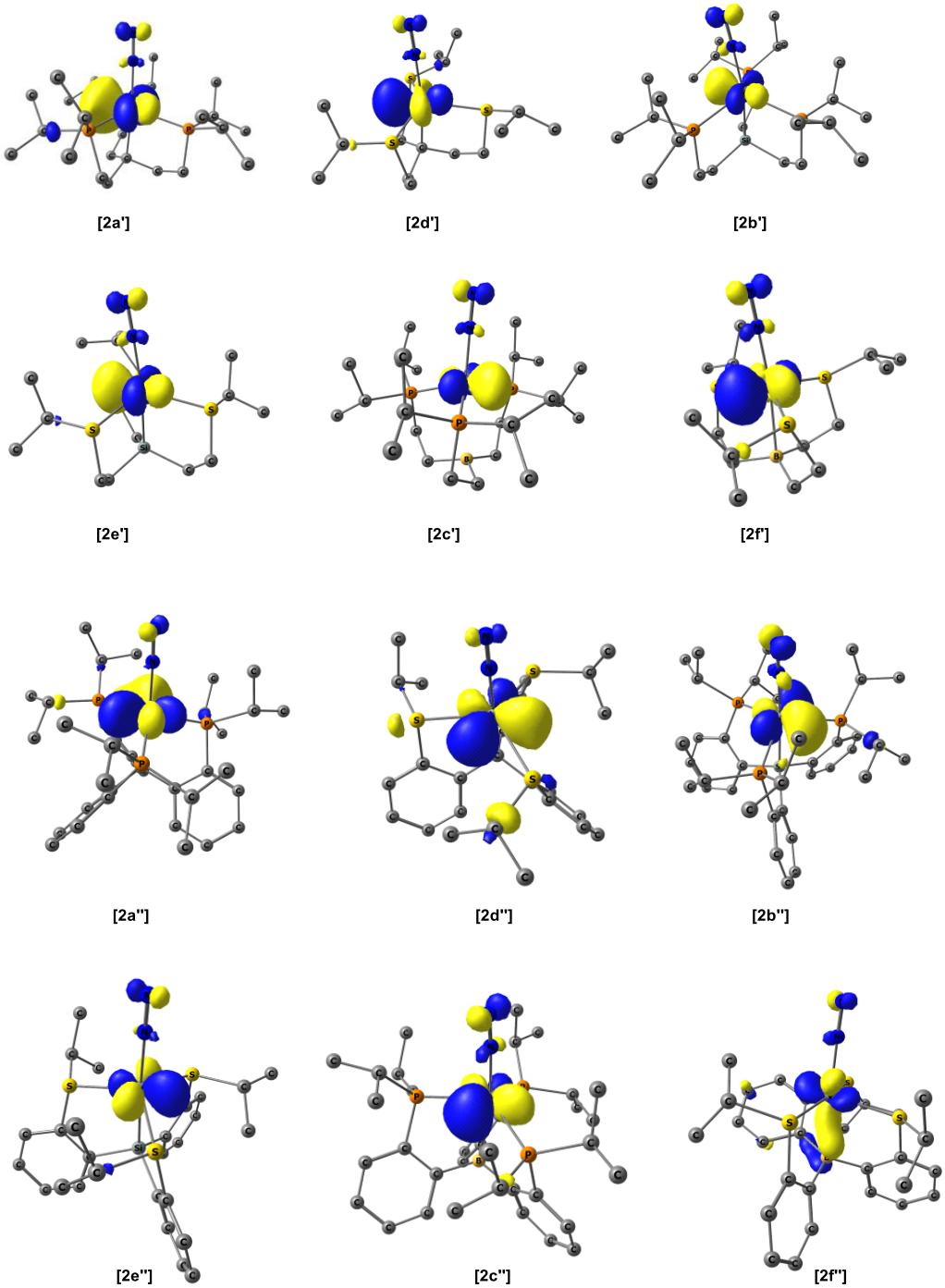

Figure 6.6: Pictorial representation of the HOMO for the dinitrogen vanadium complexes **[2a′]-[2f′]** and **[2a′′]-[2f′′]**. Hydrogen atoms of the methyl groups are omitted for clarity.

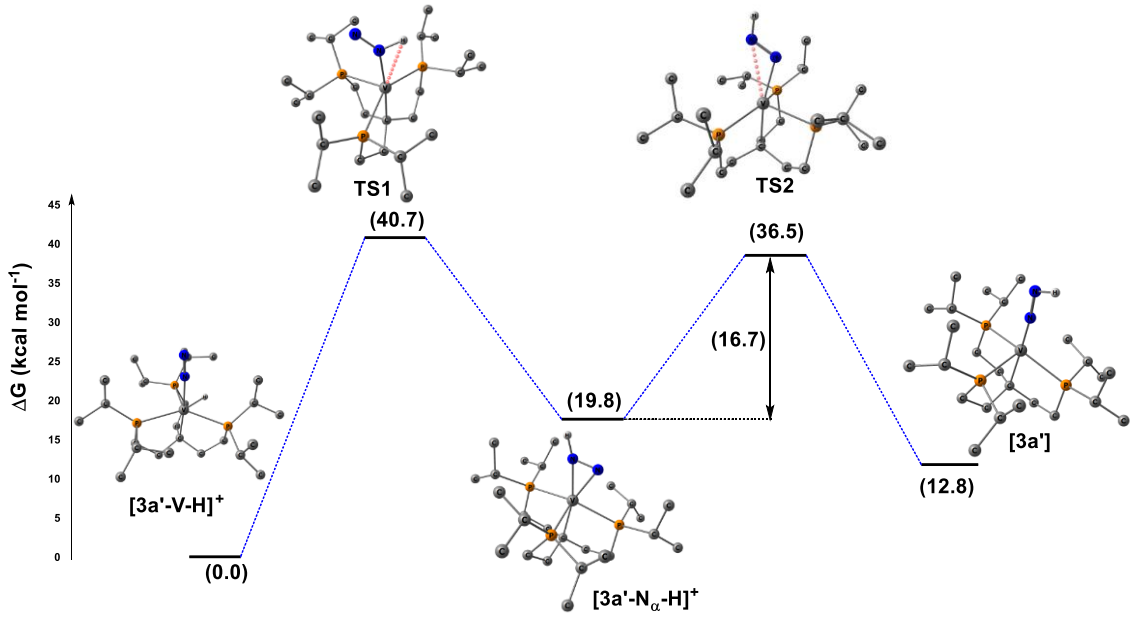

Figure 6.7: Reaction profile diagram for the conversion **[3a′-V-H]**$^{+}$ to **[3a′]** at M06-L-D3(heptane)/6-311+G* level of theory. Hydrogen atoms of the methyl groups are omitted for clarity. The energy values are in kcal mol^{-1}.

from **[2]** is the direct protonation at the distal nitrogen atom. Following this, **[3a′]** undergoes reduction to form the neutral diazenido complex **[4a′]**, in which the N–N bond is further activated as evident from the calculated N–N bond length (1.239 Å) and stretching frequency (1543.1 cm^{-1}). The diazenido complex **[4]** with carbon/silicon and boron as the bridgehead groups compute the quartet and quintet as their ground states respectively.

Table 6.5: Calculated activation energy barrier (in kcal mol^{-1}) for the transition states **TS1** and **TS2** and reaction free energy (in kcal mol^{-1}) for the formation of the intermediate involved in the formation of the **[3]** from the metal protonated vanadium complexes **[3-V-H]**$^{+}$. The reaction free energies were evaluated with respect to the metal protonated species.

Molecules	$\Delta G^{\ddagger}_{TS1}$	ΔG_{Int}	$\Delta G^{\ddagger}_{TS2}$	Molecules	$\Delta G^{\ddagger}_{TS1}$	ΔG_{Int}	$\Delta G^{\ddagger}_{TS2}$
a′	40.7	19.8	36.5	**a″**	41.7	17.7	34.8
b′	40.9	17.5	33.6	**b″**	41.3	14.1	28.7
c′	40.0	16.0	25.9	**d″**	40.0	21.6	29.2
d′	40.0	22.0	25.8	**c″**	38.5	18.1	31.8
e′	43.1	22.9	30.2	**e″**	41.9	17.6	36.7
f′	47.5	22.8	35.4	**f″**	41.9	21.1	30.4

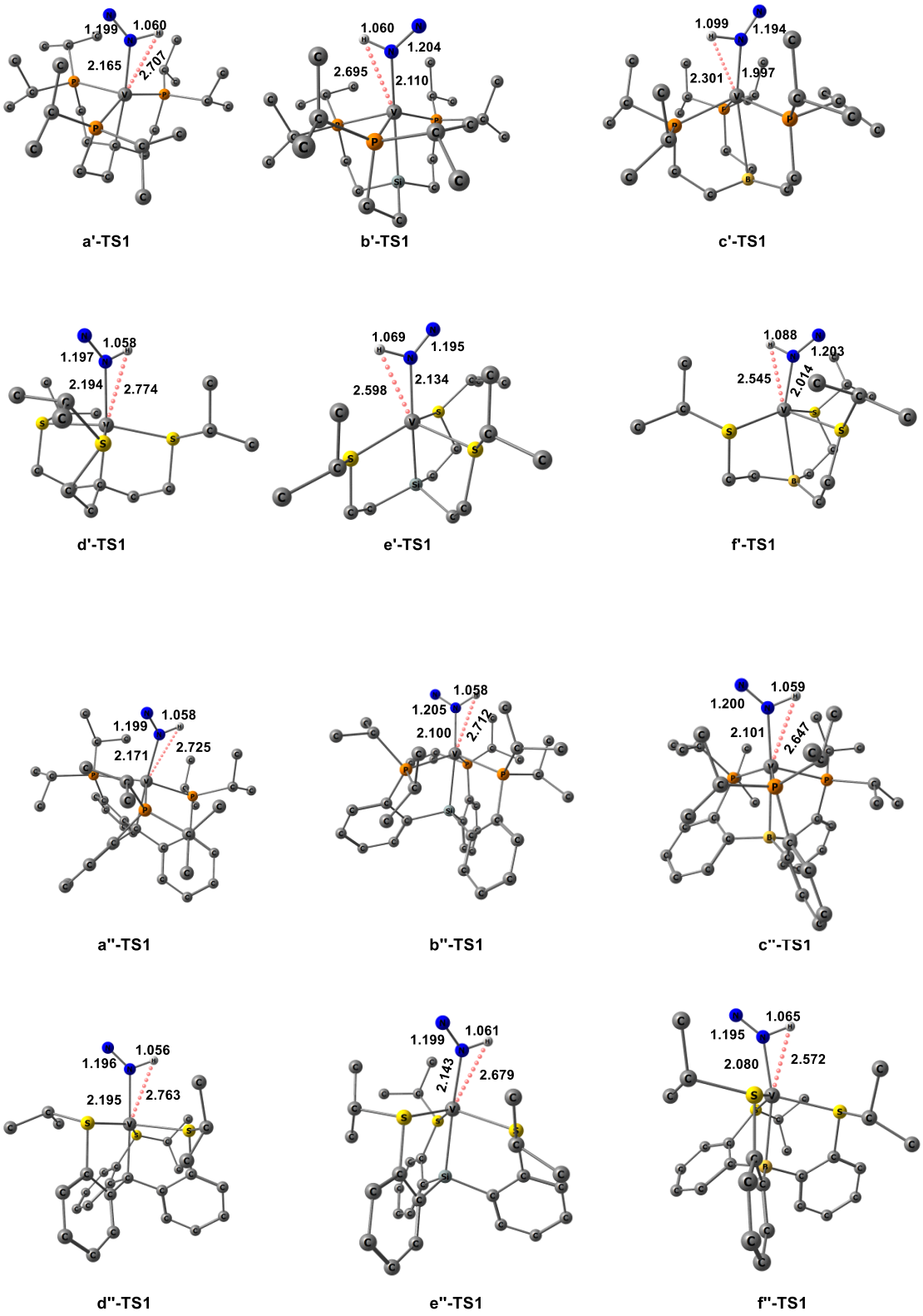

Figure 6.8: Optimized geometries of the transition state (TS1) involved in the formation of the η^2-intermediate from the metal protonated species **[3-V-H]**$^+$ of **[1a′]-[1f′]** and **[1a′′]-[1f′′]** at M06-L-D3(heptane)/6-311+G* level of theory. Hydrogen atoms of the methyl groups are omitted for clarity. Bond lengths are given in Å.

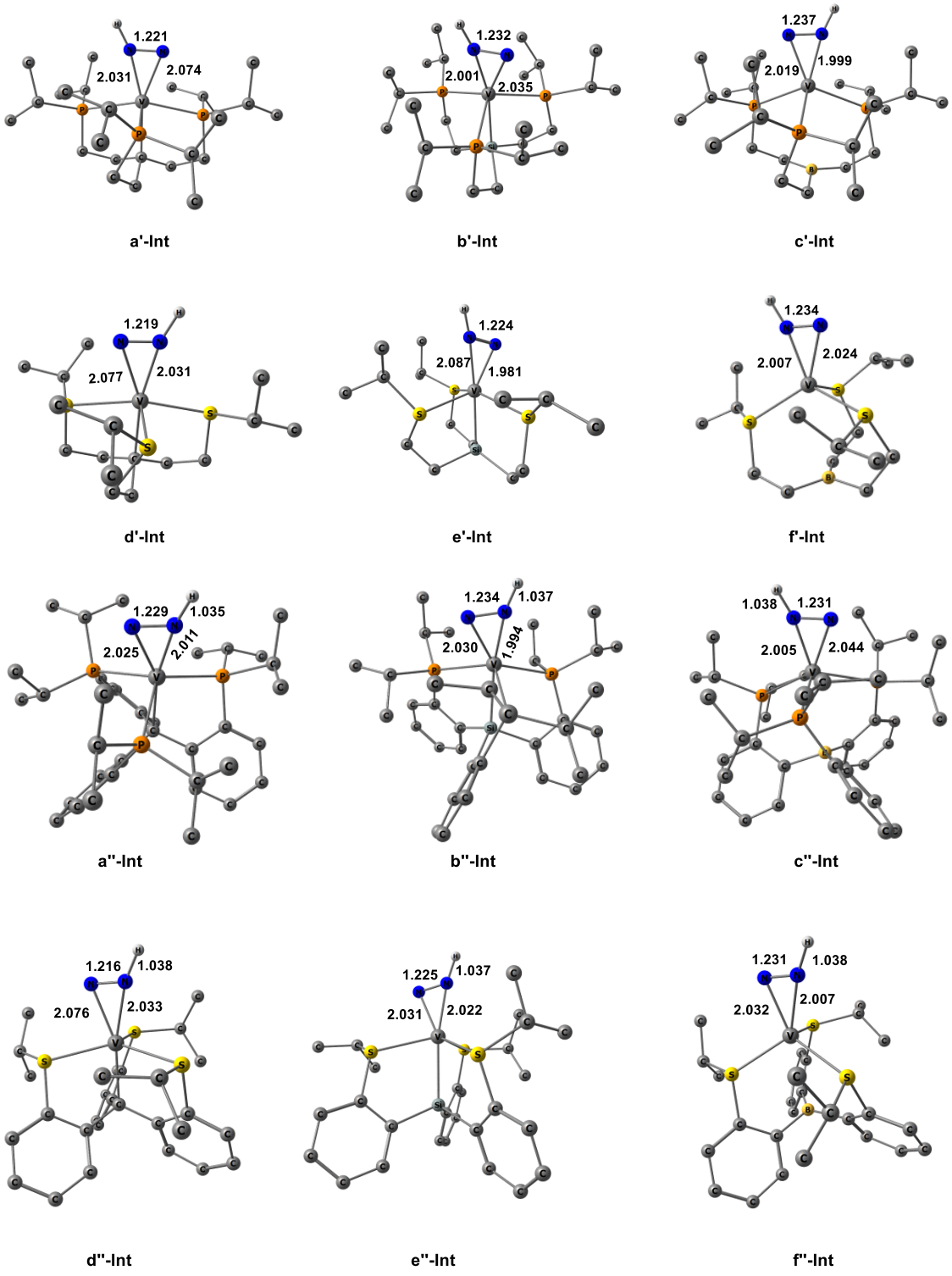

Figure 6.9: Optimized geometries of the η^2- intermediate involved in the formation of **[3]** from the metal protonated species **[3-V-H]**$^+$ of **[1a′]-[1f′]** and **[1a′′]-[1f′′]** at M06-L-D3(heptane)/6-311+G* level of theory. Hydrogen atoms of the methyl groups are omitted for clarity. Bond lengths are given in Å.

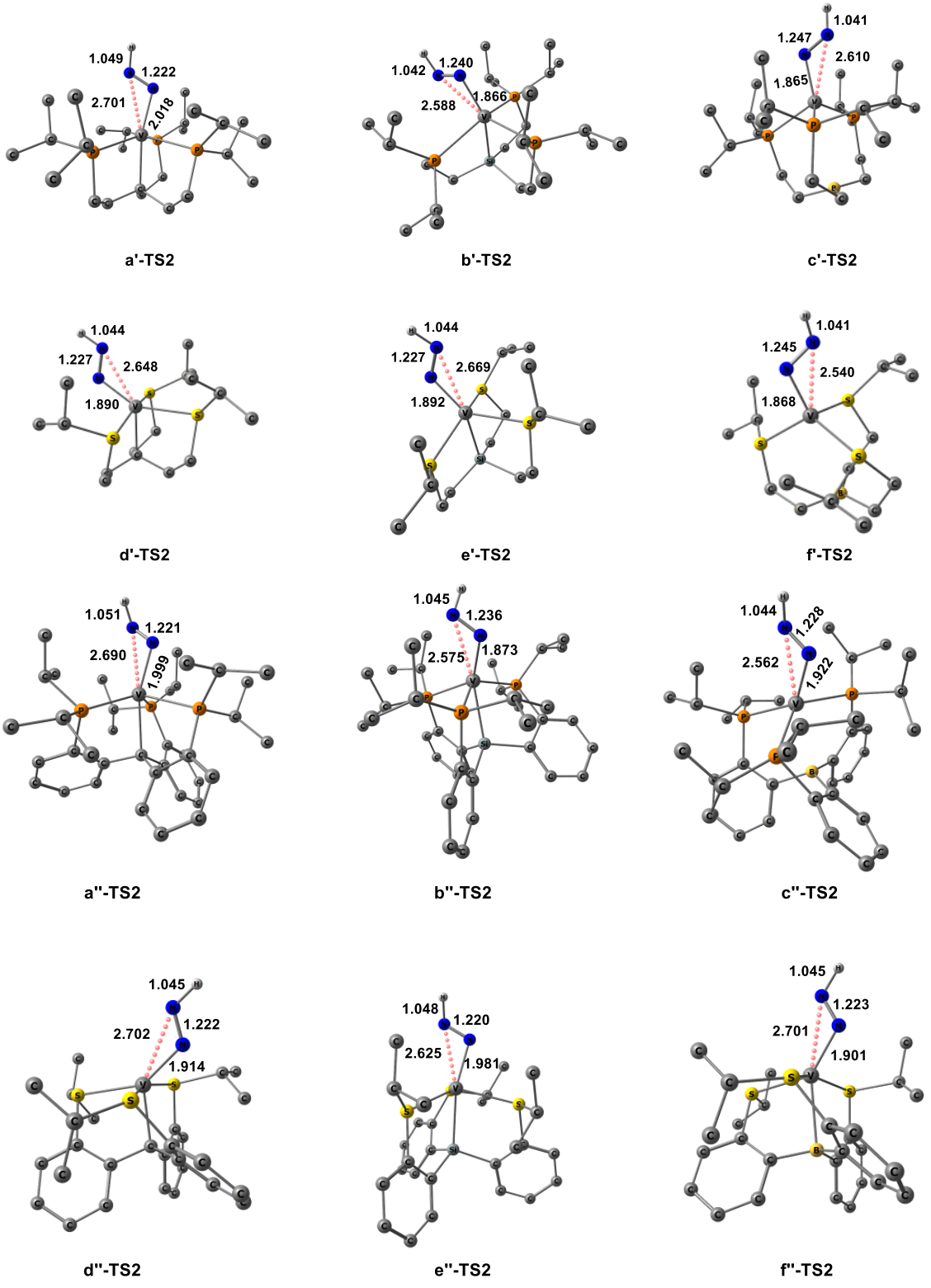

Figure 6.10: Optimized geometries of the transition state (TS2) involved in the formation of **[3]** from the η^2- intermediate of **[1a′]-[1f′]** and **[1a′′]-[1f′′]** at M06-L-D3(heptane)/6-311+G* level of theory. Hydrogen atoms of the methyl groups are omitted for clarity. Bond lengths are given in Å.

[6.3.2] Formation of the nitride complex:

Another important step in the N_2 reduction chemistry is the protonation of the neutral diazenido complex (**4**), which results in further elongation and polarization of the N–N bond. The protonation of the neutral diazenido complex may take place either at the N_β or N_α atom, leading to two different pathways viz., alternating (or symmetric) and distal (or asymmetric) pathways [60]. In the alternating pathway, the protons are added alternately to the N_α and N_β atoms. On the other hand, in the distal pathway, the first three protons are consecutively added to the distal nitrogen atom, thereby generating the first equivalent of NH_3 and a nitride complex. Thereafter, the addition of the next three protons to the N_α atom produces the second equivalent of NH_3 along with the free catalyst. Therefore, in the distal pathway, the formation of the nitride complex is one of the most crucial steps, which not only breaks the N–N bond but also generates the first equivalent of NH_3 [61]. Accordingly, in order to further investigate the potential of the proposed tripodal vanadium complexes, we have studied their efficiency towards the formation of the vanadium nitride complex by employing the following equation (Scheme 6.3). The calculated reaction free energies obtained for the generation of the

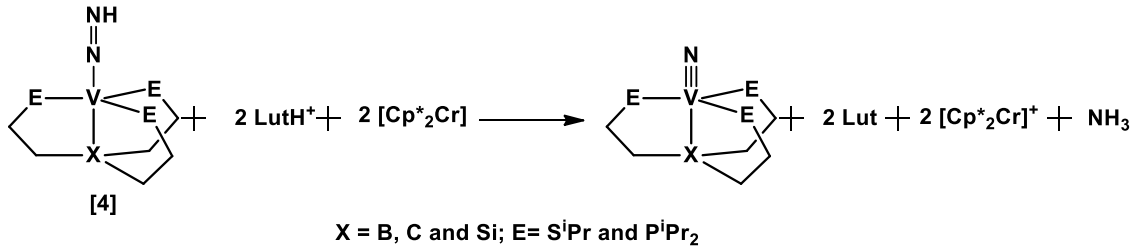

Scheme 6.3: Schematic representation of the reaction involved in the formation of vanadium nitride from the diazenido complex.

vanadium nitride complex as well as the release of the first equivalent of ammonia from the respective diazenido complexes (**[4]**) were found to be substantially exergonic (-70.8 to -84.6 kcal mol^{-1}, Table 6.6) thereby indicating their potential toward NRR. Furthermore, the calculated V≡N bond lengths for the vanadium-nitride complexes lie within the range of 1.575–1.593 Å, which were found to be comparable to experimentally observed V≡N bond lengths (1.578 Å) [62]. In addition, the calculated WBI values (2.670-2.876, Table 6.7) further corroborate the presence of a triple bond between vanadium and nitrogen. The key frontier molecular orbitals involved in the formation of the V≡N bond for the vanadium-nitride complex of **[1c′′]** (**[8c′′]**$_{dis}$) are shown in Figure 6.11 as a representative example. An analysis of these frontier orbitals

Table 6.6: Reaction free energies (ΔG, in kcal mol^{-1}) obtained for the formation of the vanadium nitride complexes from the diazenido complexes **[4]**.

Molecules	ΔG	Molecules	ΔG
[4a′]	-77.3	**[4a″]**	-75.4
[4b′]	-73.2	**[4b″]**	-70.8
[4c′]	-80.9	**[4c″]**	-75.3
[4d′]	-82.5	**[4d″]**	-76.1
[4e′]	-81.3	**[4e″]**	-74.1
[4f′]	-84.6	**[4f″]**	-81.1

Table 6.7: Calculated (M06-L-D3(heptane)/6-311+G*) important geometrical parameters for the vanadium-nitride complex ($[8]_{dis}$) of **[1a′]-[1f′]** and **[1a″]-[1f″]**. Bond lengths are given in Å and WBI values are given within parenthesis. (X = B, C and Si)

Molecules	V≡N	V-X	Molecules	V≡N	V-X
a′	1.592 (2.774)	2.307 (0.568)	**a″**	1.593 (2.670)	2.610 (0.183)
b′	1.593 (2.768)	2.551 (0.727)	**b″**	1.591 (2.759)	2.493 (0.717)
c′	1.587 (2.722)	3.022 (0.140)	**c″**	1.580 (2.713)	2.644 (0.199)
d′	1.583 (2.837)	2.179 (0.602)	**d″**	1.584 (2.850)	2.240 (0.475)
e′	1.583 (2.870)	2.488 (0.816)	**e″**	1.579 (2.876)	2.467 (0.789)
f′	1.580 (2.838)	2.568 (0.236)	**f″**	1.575 (2.871)	2.570 (0.232)

reveal that the HOMO-2 represents the formation of the σ-bond by overlap of vanadium $3d_z^2$ with $2p_z$ of nitrogen whereas HOMO-3 (V $3d_{xz}$/N $2p_x$) and HOMO-4 (V $3d_{yz}$/N $2p_y$) correspond to the two π bonds between vanadium and nitrogen atoms.

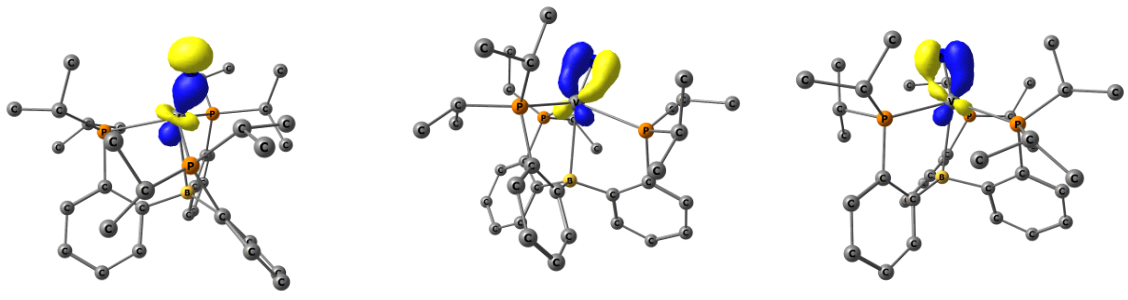

HOMO-2 HOMO-3 HOMO-4

Figure 6.11: Key frontier orbitals of the vanadium-nitride complex $[8c'']_{dis}$ corresponding to the formation of one σ and two π bonds between vanadium and nitrogen atom. The hydrogen atoms of the methyl groups are omitted for clarity.

[6.3.3] Release of hydrazine

Another side reaction that competes during the nitrogen reduction process is the formation of hydrazine. For example, Peters and coworkers reported the formation of a trace amount of hydrazine upon treatment of their iron catalyst with the reductant and proton source [24, 63]. Similarly, some of the catalysts reported by Nishibayashi and coworkers also produce hydrazine as a side product during the NRR [34, 64]. However, our calculations suggest that the proposed vanadium complexes are unlikely to generate hydrazine (Scheme 6.4) as a side product during the nitrogen reduction process, which is reflected in the endergonicity (11.2 to 17.7 kcal mol^{-1}, Table 6.8) associated with the release of hydrazine from the vanadium-hydrazine complexes. Furthermore, the reaction

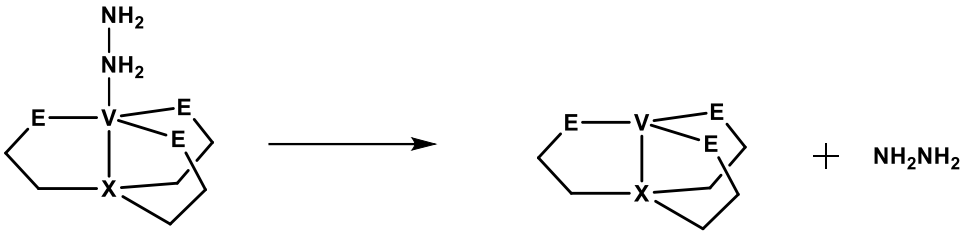

X = B, C and Si ; E= S^{i}Pr and P^{i}Pr$_2$

Scheme 6.4: Schematic representation of the reaction involved in the release of hydrazine from the vanadium-hydrazine complex.

free energy obtained for Schrock's vanadium complex (**II**) suggests that it is slightly endergonic in nature (9.7 kcal mol^{-1}). This perhaps explain why no hydrazine was detected upon treatment of the complex **II** with proton source and reductant.

Table 6.8: Reaction free energies (ΔG, in kcal mol^{-1}) obtained for the release of hydrazine from the vanadium-hydrazine complex of the proposed vanadium complexes and Schrock's vanadium complex (**II**).

Molecules	ΔG	Molecules	ΔG
[1a′]	14.8	**[1a″]**	15.7
[1b′]	17.2	**[1b″]**	11.2
[1c′]	14.8	**[1c″]**	14.8
[1d′]	15.9	**[1d″]**	16.0
[1e′]	15.4	**[1e″]**	17.7
[1f′]	15.4	**[1f″]**	16.8
II	9.7		

Further, it is to be noted that all the complexes under consideration compute almost similar energetics for the key steps of NRR studied so far. Therefore, it may be expected that the effect of the bridgehead atom (X = B, C and Si) is negligible. Indeed, the energetics computed for different steps employing B/C/Si as the bridgehead atom deviate from each other by less than 10 kcal mol^{-1} (Table 6.3, Table 6.6 and Table 6.8). Therefore, we decided to study the full catalytic cycle by considering boron anchored complexes **[1c″]** and **[1f″]** as representative examples. The motivation for choosing boron as the bridgehead group came from the experimental works of Peters and coworkers, who have reported higher activity of the boron-containing iron catalyst in the dinitrogen reduction process [23, 26, 65-66].

[6.3.4] Nitrogen reduction reaction (NRR) with [1c″]

As discussed above, the catalyst **[1c″]** favors the generation of the diazenido complex **[4c″]** (Table 6.3). The complex **[4c″]** thus formed is susceptible to further protonation as it features two lone pairs of electrons localized at the N_α and N_β atoms. Protonation at N_α or N_β atoms of **[4c″]** generate the cationic complexes $\mathbf{[5c'']_{alt}}$ (in a quintet ground state) and $\mathbf{[5c'']_{dis}}$ (in a triplet ground state), respectively, thereby bifurcating the catalytic cycle into two different pathways viz., alternating and distal pathways (Scheme 6.5 and Figure 6.12). The reaction free energies obtained for the formation of the nitrogenous species $\mathbf{[5c'']_{alt}}$ and $\mathbf{[5c'']_{dis}}$ are computed to be -9.8 and -20.6 kcal mol^{-1} respectively (Figures 6.13 and 6.15). Therefore, from the thermodynamic point of view, it may be inferred that for the vanadium catalyst **[1c″]**, the distal pathway may be preferred to the alternating pathway. In addition, we have also looked for the probable TSs and intermediates involved during this transformation process. Indeed, for the alternating pathway, we

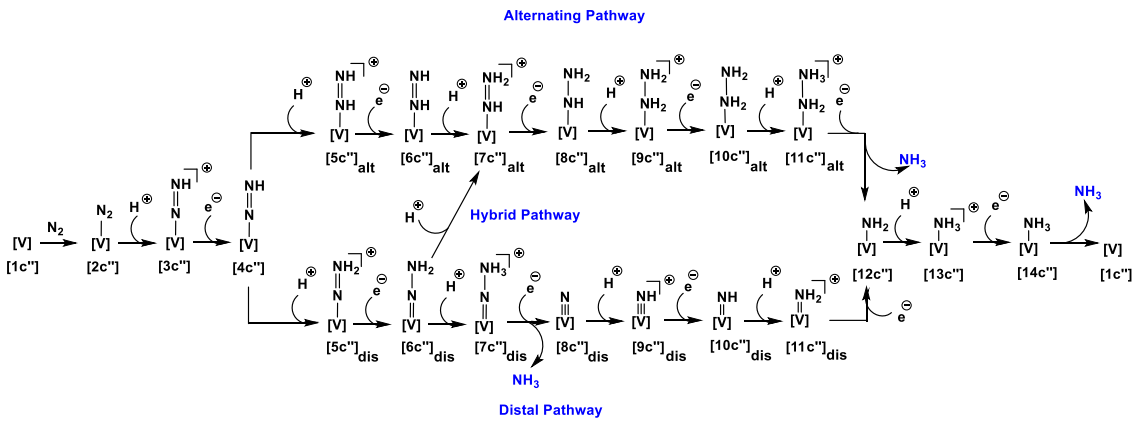

Scheme 6.5: Alternating, hybrid and distal pathways for dinitrogen reduction to NH_3.

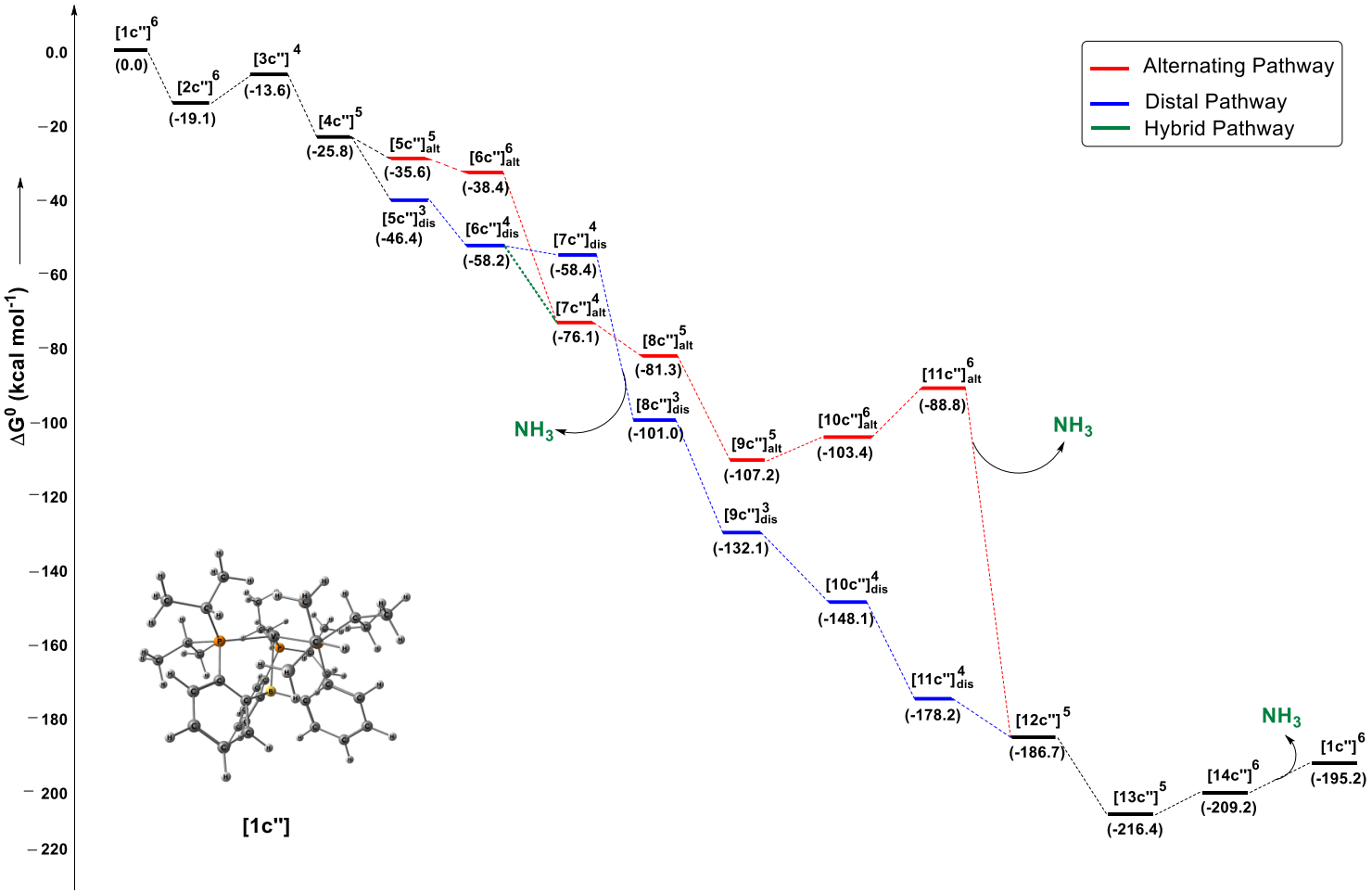

Figure 6.12: Energy profile diagram for the reduction process of N_2 to NH_3 mediated by the catalyst **[1c′′]**. The energy values are given in kcal mol^{-1} and calculated at M06-L-D3(heptane)/6-311+G* level of theory. The superscript outside the bracket indicate the spin state of the species.

could locate an intermediate that formed upon protonation at the metal center (Figure 6.13). The formation of this intermediate **[4c″-V-H]**$^{+}$ was computed to be marginally exergonic (-4.5 kcal mol^{-1}) indicating that this reaction may also compete during the

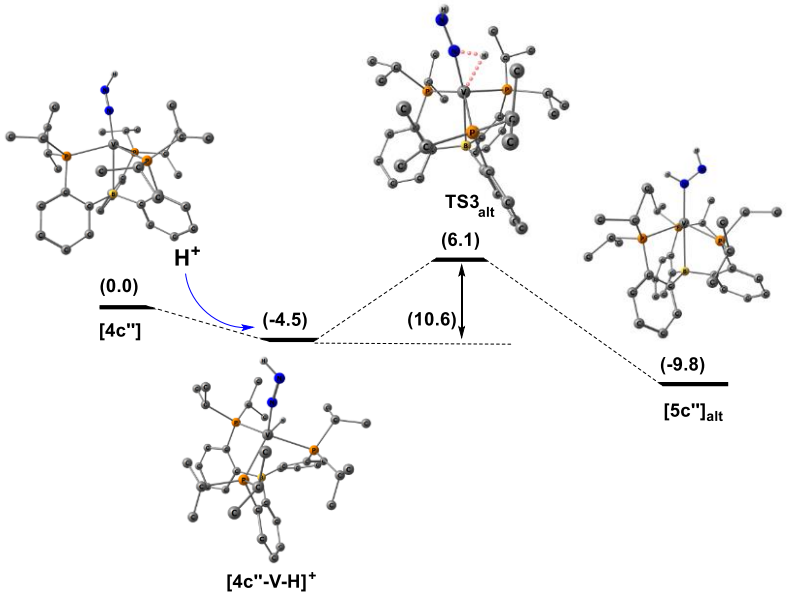

Figure 6.13: Reaction profile diagram for the conversion of **[4c″]** to **[5c″]$_{alt}$** via alternating pathway at M06-L-D3(heptane)/6-311+G* level of theory. Hydrogen atoms of the methyl groups are omitted for clarity. The energy values are in kcal mol^{-1}.

catalytic cycle. The intermediate thus formed passes through a TS (**TS3$_{alt}$**) in which the proton attached to the vanadium center migrates to the N$_{\alpha}$ atom to yield the cationic complex **[5c″]$_{alt}$**. Since the metal protonated species **[4c″-V-H]**$^{+}$ (S =1) and the complex **[5c″]$_{alt}$** (S=2) exhibit different ground state multiplicities, we located the TSs in both multiplicities (triplet and quintet), and the barrier height was computed by considering the lowest-energy TS (Figure 6.14). The activation barrier obtained (considering the triplet state TS) for this transformation process (**[4c″-V-H]**$^{+}$**→[5c″]$_{alt}$**) was computed to be 10.6 kcal mol^{-1}. However, as shown in Figure 6.15 for the conversion of **[4c″]→[5c″]$_{dis}$** via the distal pathway, we located two intermediates and two TSs. The first step, the formation of the metal protonated diazenido complex **[4c″-V-H]**$^{+}$, is common for both pathways. Thereafter, **[4c″-V-H]**$^{+}$ rearranges via a TS (**TS4′$_{dis}$**) having an activation barrier of 16.8 kcal mol^{-1} to generate another η^2-type intermediate (**η^2_{NN}-[4c″-V-H]**$^{+}$). Finally, the second intermediate proceeds through another TS (**TS4″$_{dis}$**) in which the proton attached to the metal center moves toward the distal nitrogen atom to generate **[5c″]$_{dis}$**. The barrier height obtained for the process **η^2_{NN}-[4c″-V-H]**$^{+}$**→[5c″]$_{dis}$**

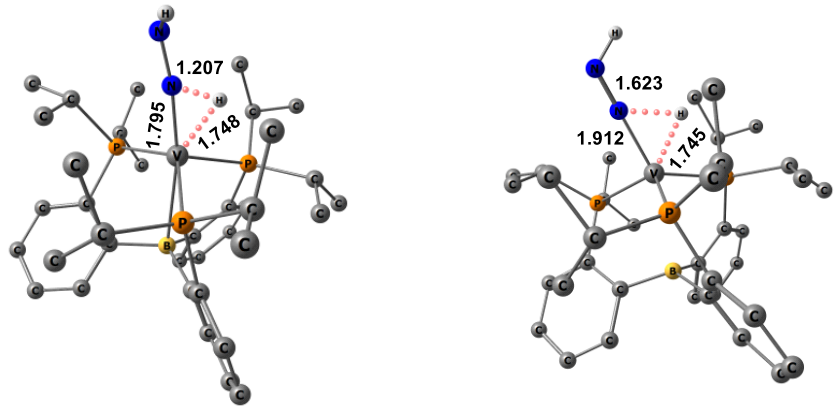

Figure 6.14: Optimized geometries of the TS (TS3) involved during conversion of **[4]→[5]$_{alt}$** in all possible spin states for the molecules **[1c′′]** at M06-L-D3(heptane)/6-311+G* level of theory. Total energy (T.E) values are given in hartree. The values given within parenthesis corresponds to the relative energy difference between the TSs. Hydrogen atoms of the methyl groups are omitted for clarity. Bond lengths are given in Å.

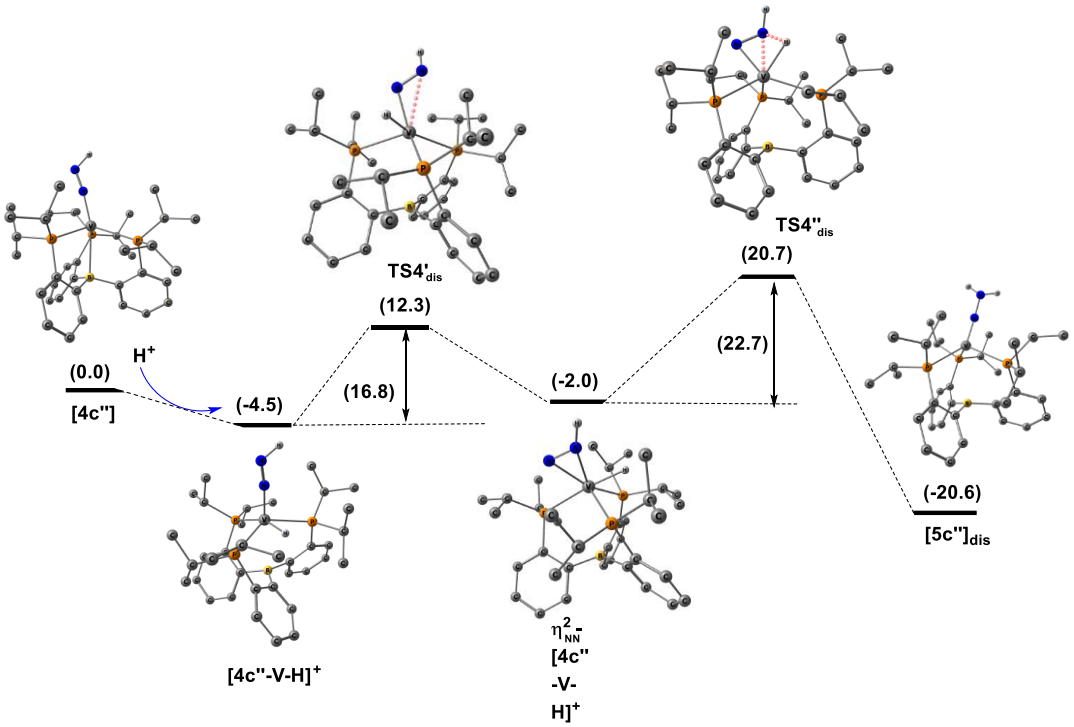

Figure 6.15: Reaction profile diagram for the conversion of **[4c′′]** to **[5c′′]$_{dis}$** via distal pathway at M06-L-D3(heptane)/6-311+G* level of theory. Hydrogen atoms of the methyl groups are omitted for clarity. The energy values are in kcal mol^{-1}.

is computed to be 22.7 kcal mol^{-1}. Therefore, from the kinetic point of view, both pathways may be feasible, and depending upon the reaction conditions, one pathway may be favored over the other. Accordingly, we have considered both pathways while studying the potential applicability of **[1c″]** in the dinitrogen reduction process.

Furthermore, it is to be noted that some of the nitrogenous species involved in the alternating and distal pathways are isomeric with one another (Scheme 6.5 and Figure 6.12). For instance, species like $\mathbf{[5c'']_{alt}}$, $\mathbf{[6c'']_{alt}}$ and $\mathbf{[7c'']_{alt}}$, which we generally encounter in the alternating pathway are isomeric to the species $\mathbf{[5c'']_{dis}}$, $\mathbf{[6c'']_{dis}}$ and $\mathbf{[7c'']_{dis}}$, respectively, of the distal pathway. Hence, there is a possibility of interconversion of these species either via a proton-catalyzed (Figure 6.16) or by a proton transfer (Figure 6.17) pathway. The calculated reaction free energies obtained for the deprotonation reactions involved in the conversion of $\mathbf{[5c'']_{alt}}$, $\mathbf{[6c'']_{alt}}$ and $\mathbf{[7c'']_{alt}}$ to $\mathbf{[5c'']_{dis}}$, $\mathbf{[6c'']_{dis}}$ and $\mathbf{[7c'']_{dis}}$, respectively, via the proton-catalyzed pathway are computed to be considerably endergonic (9.8 to 19.4 kcal mol^{-1}) in nature, thereby ruling out the possibility of such an interconversion process. Similarly, we have also located the

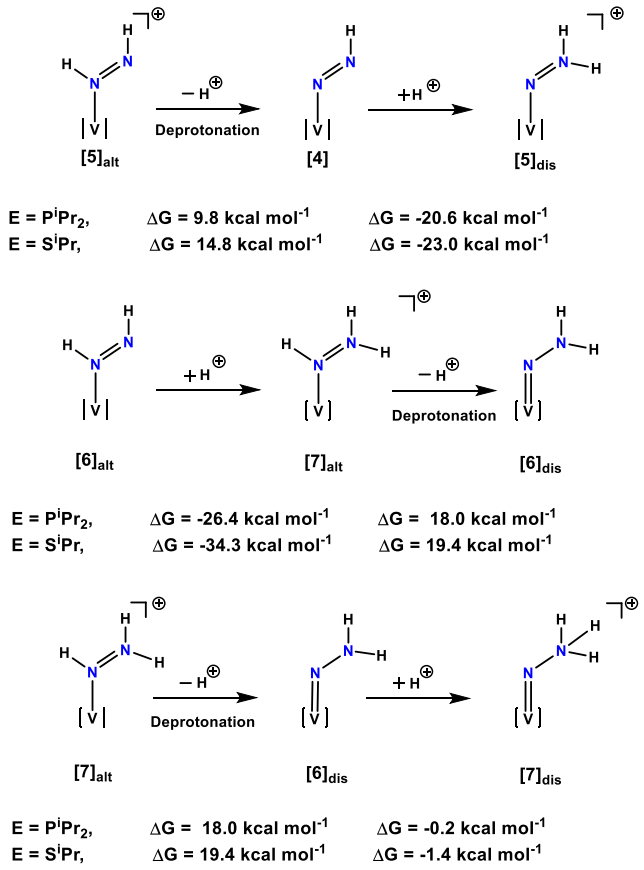

Figure 6.16: Schematic representation of the possible proton catalyzed pathways involved in the conversion of $\mathbf{[5]_{alt}}$, $\mathbf{[6]_{alt}}$ and $\mathbf{[7]_{alt}}$ to $\mathbf{[5]_{dis}}$, $\mathbf{[6]_{dis}}$ and $\mathbf{[7]_{dis}}$, respectively.

probable TSs involved in the interconversion of these isomeric species via the proton transfer pathway. The barrier heights obtained for the processes **[5c′′]$_{alt}$→[5c′′]$_{dis}$**, **[6c′′]$_{alt}$→[6c′′]$_{dis}$** and **[7c′′]$_{alt}$→[7c′′]$_{dis}$** were substantially high (34.1–49.8 kcal mol^{-1}, Figure 6.17) indicating that such transformations are unlikely to take place. Furthermore, it is important to note that for the transformations **[5c′′]$_{alt}$→[5c′′]$_{dis}$** and **[6c′′]$_{alt}$→[6c′′]$_{dis}$**, the starting reactant and the final species do not possess the same ground state

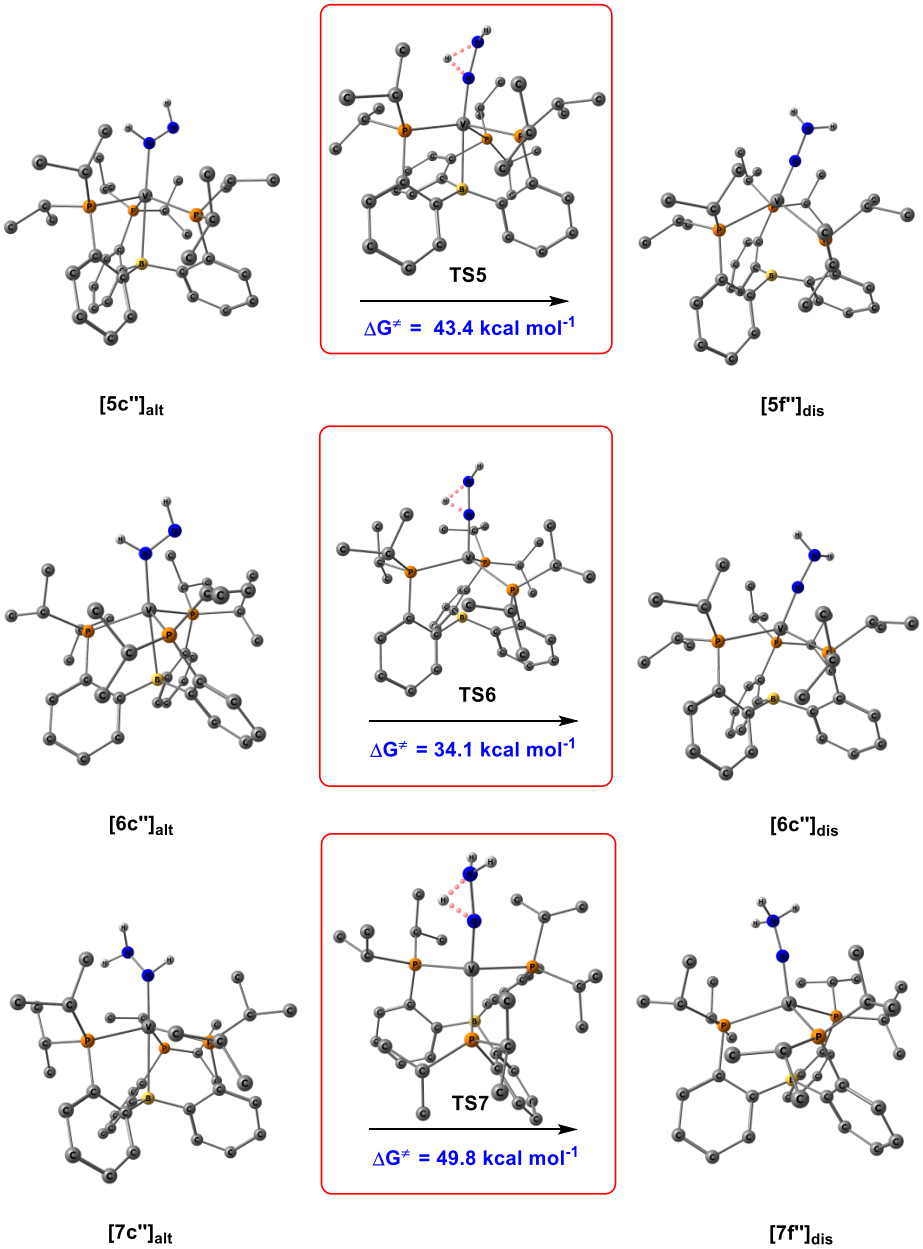

Figure 6.17: Optimized geometries of the TSs involved in the conversion of **[5c′′]$_{alt}$**, **[6c′′]$_{alt}$** and **[7c′′]$_{alt}$** to **[5c′′]$_{dis}$**, **[6c′′]$_{dis}$** and **[7c′′]$_{dis}$** respectively via proton transfer pathway at M06-L-D3(heptane)/6-311+G* level of theory. The hydrogen atoms of the methyl groups are omitted for clarity.

multiplicity. Therefore, in order to obtain the activation energy barriers associated with these conversion processes, we have located the probable TSs in all the possible spin states, and the barrier heights were computed by considering the lowest energy TS (Figures 6.18-6.19).

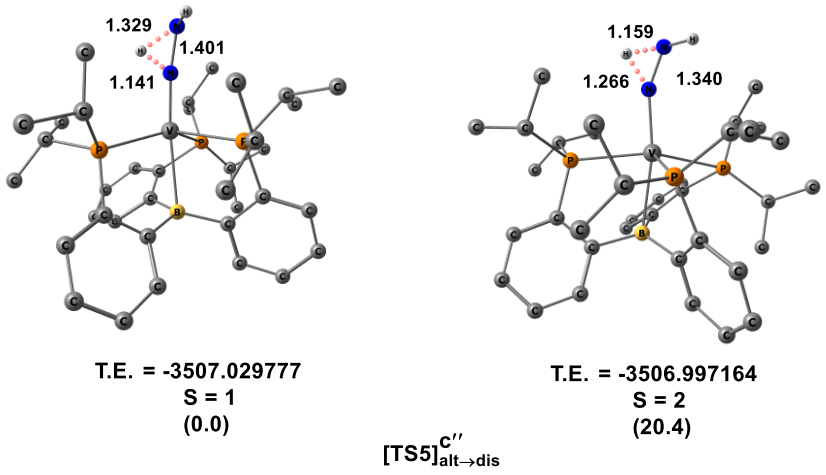

Figure 6.18: Optimized geometries of the TS (TS5) involved during conversion of **[5]$_{alt}$→[5]$_{dis}$** in all possible spin states for the molecules **[1c′′]** at M06-L-D3(heptane)/6-311+G* level of theory. Total energy (T.E) values are given in hartree. The values given within parenthesis corresponds to the relative energy difference between the TSs. Hydrogen atoms of the methyl groups are omitted for clarity. Bond lengths are given in Å.

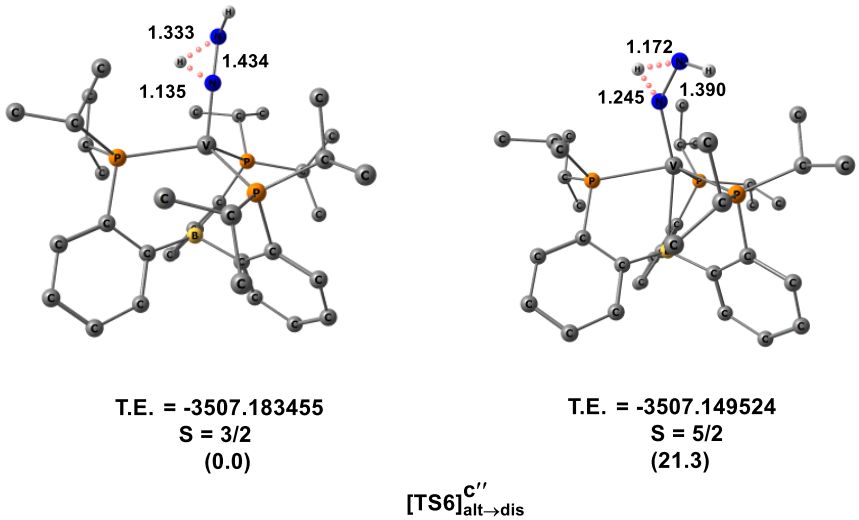

Figure 6.19: Optimized geometries of the TS (TS6) involved during conversion of **[6]$_{alt}$→[6]$_{dis}$** in all possible spin states for the molecules **[1c′′]** at M06-L-D3(heptane)/6-311+G* level of theory. Total energy (T.E) values are given in hartree. The values given within parenthesis corresponds to the relative energy difference between the TSs. Hydrogen atoms of the methyl groups are omitted for clarity. Bond lengths are given in Å.

In the alternating pathway, the species **[5c″]$_{alt}$**, which is formed upon protonation of the diazenido complex **[4c″]**, undergoes reduction to afford a neutral vanadium(0) diazene complex **[6c″]$_{alt}$**. The neutral complex **[6c″]$_{alt}$** can exhibit three different multiplicities viz., sextet, quartet and doublet with the sextet state being the most stable one. Therefore, we have considered the sextet geometry for free-energy calculation. The reaction process **[5c″]$_{alt}$→[6c″]$_{alt}$** is computed to be exergonic by -2.8 kcal mol^{-1}. The next step is the protonation of **[6c″]$_{alt}$** which generates a cationic complex **[7c″]$_{alt}$** in a quartet state, and this process is highly exergonic (-37.7 kcal mol^{-1}). Further reduction of **[7c″]$_{alt}$**, followed by protonation of the resulting complex **[8c″]$_{alt}$** in a quintet ground state, generates a cationic vanadium(I) hydrazine complex **[9c″]$_{alt}$** with no change in multiplicity. Both of these reaction processes i.e. conversion of **[7c″]$_{alt}$→[8c″]$_{alt}$** and **[8c″]$_{alt}$→[9c″]$_{alt}$** were computed to be exergonic by -5.2 kcal mol^{-1} and -25.9 kcal mol^{-1}, respectively. We observed a gradual elongation of the N–N bond length all the way from the species **[5c″]$_{alt}$** (1.278 Å) to **[9c″]$_{alt}$** (1.444 Å), indicating the activation of the dinitrogen molecule. Reduction of **[9c″]$_{alt}$** requires 3.8 kcal mol^{-1} to generate the neutral vanadium(0) hydrazine complex **[10c″]$_{alt}$**, with a sextet ground state. At this point of the catalytic cycle, the complex **[10c″]$_{alt}$** thus formed may either undergo further protonation or it can release hydrazine (N_2H_4) as a side product via the dissociation of the V–N_α bond. However, as mentioned earlier, the species **[10c″]$_{alt}$** shows a lower propensity to release N_2H_4, which is evident from the endergonicity associated with the release of N_2H_4 from the vanadium(0) hydrazine complex (14.8 kcal mol^{-1}, Table 6.8). However, it should be noted that further protonation of **[10c″]$_{alt}$** also demands an energy of 14.6 kcal mol^{-1} to yield the cationic complex **[11c″]$_{alt}$** in a sextet ground state. The endergonicity associated with this reduction step may be traced to the higher stability of the lone pair located at the distal nitrogen atom (E_{LP} = -6.7 eV, Figure 6.20). However, the substantial exergonicity (-97.9 kcal mol^{-1}) of the next reduction step, i.e. the conversion of **[11c″]$_{alt}$→[12c″]** along with the release of the first equivalent of ammonia, may act as a driving force for the overall conversion of **[10c″]$_{alt}$** to **[12c″]** in a quintet ground state. Furthermore, it should be noted that the distal pathway is also a viable route for obtaining the vanadium(I) amide species **[12c″]**. Therefore, both the pathways (alternating and distal) that were bifurcated at **[4c″]**, again merge at this point. Such

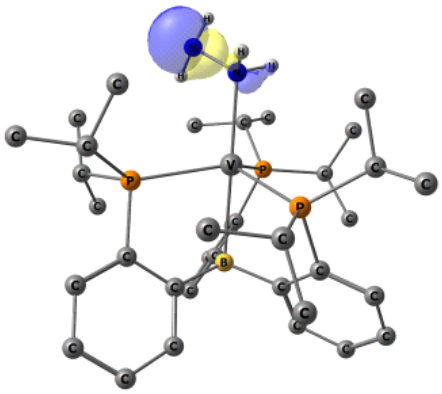

HOMO-13
E_{LP} = -6.7 eV

$[10c'']_{alt}$

Figure 6.20: Molecular orbital showing the presence of amino lone pair on the β-nitrogen atom of the complex **$[10c'']_{alt}$**. The hydrogen atoms of the methyl groups are omitted for the sake of clarity.

vanadium amide complexes ([V]-NH_2) are known experimentally [34, 37], and are believed to be one of the key intermediates involved during the latter stage of the dinitrogen reduction process.

As mentioned above, in the distal pathway, the protons are successively added to the distal nitrogen atom. In the first step of the distal pathway, the species **$[5c'']_{dis}$** that is formed upon protonation at the distal nitrogen atom of **[4c″]** undergoes reduction to generate a neutral hydrazido complex **$[6c'']_{dis}$** in a quartet ground state. The reaction free energy computed for this reduction process is -11.8 kcal mol^{-1}. Very recently, Hu and coworkers also reported the isolation and characterization of such a vanadium-hydrazido complex ([V]=NNH_2) [37], indicating the possibility of the formation of the complex **$[6c'']_{dis}$** during NRR. The species **$[6c'']_{dis}$** bears two lone pairs of electrons and hence should undergo further protonation. Indeed, protonation of **$[6c'']_{dis}$** at the distal nitrogen atom generates a cationic species **$[7c'']_{dis}$** with a quartet ground state, and the process was computed to be slightly exergonic in nature (-0.26 kcal mol^{-1}). The species **$[7c'']_{dis}$** features a substantially elongated N–N bond length (1.407 Å) indicating considerable activation of the dinitrogen molecule (free N≡N bond length = 1.101 Å, *ca.* at the same level of theory). Reduction of **$[7c'']_{dis}$** led to splitting of the N–N bond, generating the first equivalent of NH_3 and a nitride complex **$[8c'']_{dis}$** in a triplet ground state. This reduction step is computed to be highly exergonic in nature (-42.8 kcal mol^{-1}). It is

interesting to note that the reduction step that led to the generation of the first equivalent of NH_3 in the alternating pathway (**[11c′′]$_{alt}$→[12]**) is computed to be hugely exergonic (more than two times) compared to that of the distal pathway (**[7c′′]$_{dis}$→[8c′′]$_{dis}$**). The higher exergonicity associated with the release of the first equivalent of NH_3 in the alternating pathway (-97.9 kcal mol^{-1}) may be attributed to the higher degree of activation of the N–N bond (1.469 Å, WBI = 0.772) in **[11c′′]$_{alt}$** (N–N bond length in **[7c′′]$_{dis}$**: 1.407 Å; WBI: 1.018). **[8c′′]$_{dis}$** features a triple bond between the vanadium and nitrogen atoms (V≡N bond length in **[8c′′]$_{dis}$**: 1.580 Å; WBI: 2.713), and also a lone pair of electrons localized at the nitrogen atom (Figure 6.21). **[8c′′]$_{dis}$** readily undergoes protonation, generating **[9c′′]$_{dis}$** without any change in the spin state, and this process is

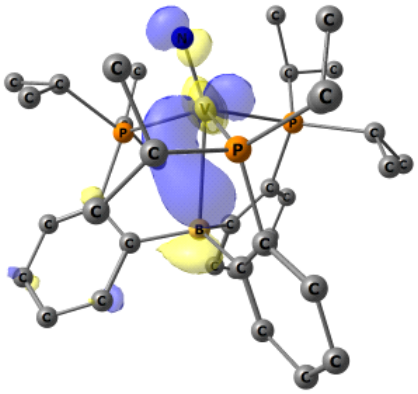

Figure 6.21: Molecular orbital showing the presence of lone pair on the nitrogen atom of the complexes **[8c′′]$_{dis}$**. The hydrogen atoms of the methyl groups are omitted for the sake of clarity.

computed to be substantially exergonic by -31.1 kcal mol^{-1}. Reduction of the species **[9c′′]$_{dis}$** and the protonation of the ensuing complex **[10c′′]$_{dis}$** in a quartet state generates the complex **[11c′′]$_{dis}$** with no change in multiplicity. These two reaction processes were computed to be considerably exergonic by -16.0 and -30.1 kcal mol^{-1}, respectively. The next reduction step, i.e., the conversion of **[11c′′]$_{dis}$** to neutral vanadium(I) amide species **[12c′′]**, is exergonic as well (-8.5 kcal mol^{-1}). All the species involved in the distal pathway exhibit a TBP geometry around the metal center. In addition, NBO analysis suggests the presence of multiple bonds between vanadium and nitrogen in most of the nitrogenous species involved in the distal pathway. Furthermore, in an experimental

study, Peters and coworkers demonstrated the viability of another pathway, viz., a hybrid distal-to-alternating pathway, that may also operate during the nitrogen reduction process [63]. Indeed, the reaction free energy obtained for the transformation of **[6c″]$_{dis}$→[7c″]$_{alt}$** is quite exergonic by -18.1 kcal mol^{-1}, indicating that such a hybrid pathway may also be feasible during the nitrogen reduction process.

The final three steps of the catalytic cycle are common for both pathways. Protonation of **[12c″]** affords a cationic complex **[13c″]** in a quintet ground state (the singlet and triplet states are higher in energy by 33.0 and 8.5 kcal mol^{-1}, respectively). This protonation process is calculated to be considerably exergonic by -29.7 kcal mol^{-1}. However, reduction of **[13c″]** to generate **[14c″]** is calculated to be endergonic by 7.2 kcal mol^{-1}. The last step of the catalytic cycle is a key one, as it leads to the regeneration of the catalyst **[1c″]**, and release of the second equivalent of ammonia. This process is computed to be endergonic by 14.0 kcal mol^{-1}. Similar energetics were also obtained for this last step, employing Schrock's molybdenum catalyst (**I**) by Reiher (27.7 kcal mol^{-1}) [16] and Tuczek (8.8 kcal mol^{-1}) [15]. At this point of the catalytic cycle, **[1c″]** again needs to bind with dinitrogen to restart the nitrogen reduction process. Gratifyingly, the reaction free energy associated with the binding of N_2 with **[1c″]** is an exergonic process (-19.1 kcal mol^{-1}, Table 6.3). Therefore, the overall NH_3 and N_2 exchange process for the catalyst **[1c″]** is computed to be exergonic by -5.0 kcal mol^{-1}. Hence, from the above discussion, it can be inferred that the proposed vanadium catalyst **[1c″]** may be considered a promising system for the nitrogen reduction reaction, which is not only evident from the highly exergonic calculated reaction free energies of different steps but also from the thermally surmountable, moderate barrier heights associated with these steps.

Furthermore, we have also studied the full catalytic cycle by employing the catalyst **[1f″]** (bearing S^{i}Pr as the equatorial group). The energy profile diagram for the conversion of N_2 to NH_3 mediated by **[1f″]** is given in Figure 6.22 and the energetics were found to be comparable to that obtained using **[1c″]**. For example, release of the first equivalent of NH_3 along the distal and alternate pathways was calculated to be exergonic by -43.5 and -97.2 kcal mol^{-1}, respectively, which are comparable to those obtained for **[1c″]** (-42.8 and -97.9 kcal mol^{-1} respectively). Akin to the catalyst **[1c″]**, we have also studies the viability of the alternate and distal modes of protonation during

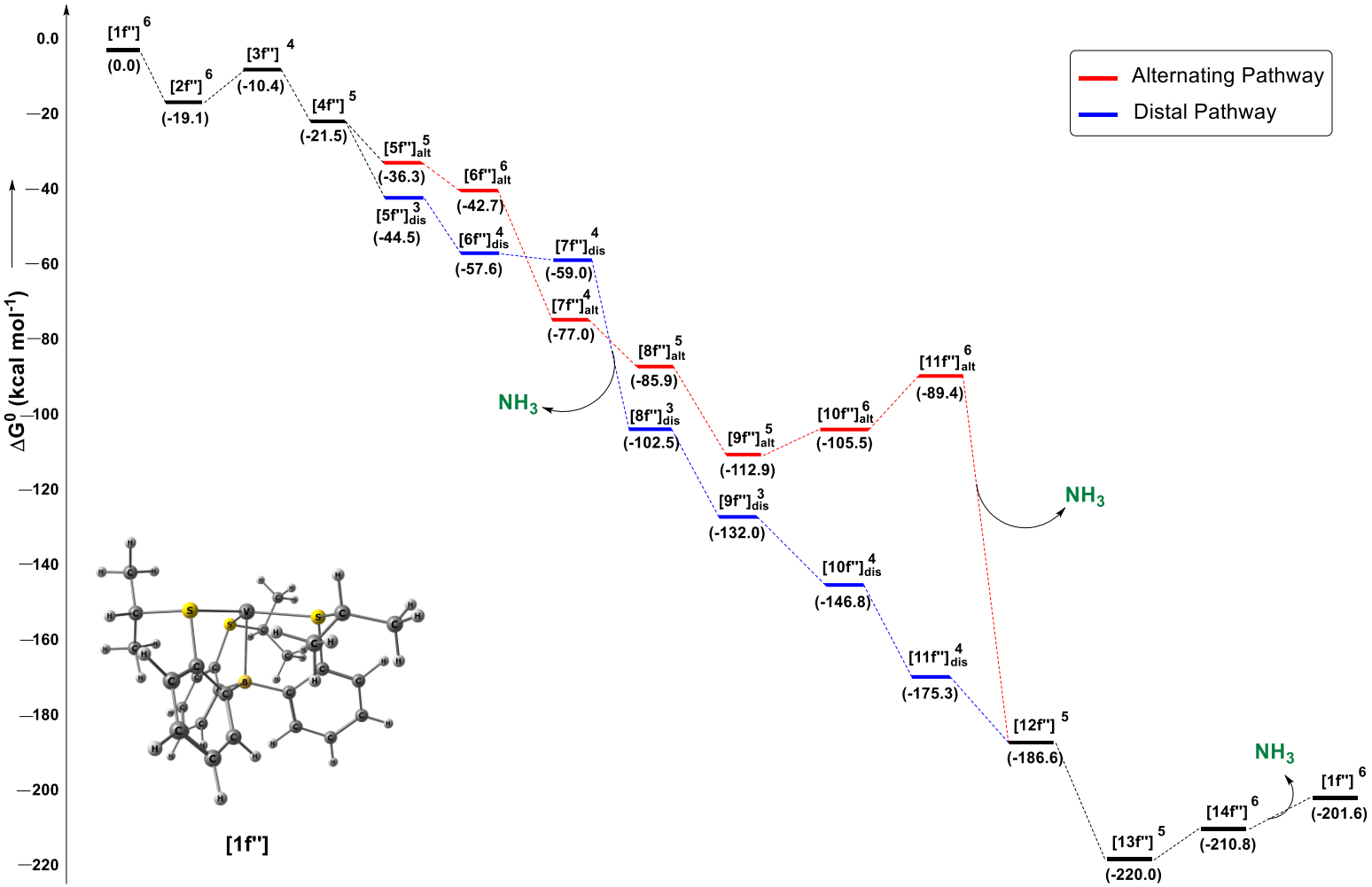

Figure 6.22: Energy profile diagram for the reduction process of N_2 to NH_3 mediated by the catalyst **[1f′′]**. The energy values are given in kcal mol^{-1} and calculated at M06-L-D3(heptane)/6-311+G* level of theory. The superscript outside the bracket indicate the spin state of the species.

the nitrogen reduction process for the catalyst **[1f″]** (Figures 6.23-6.24). It is evident from Table 6.3 that the formation of the diazenido complex (**[4f″]**) for **[1f″]** is thermodynamically feasible. Protonation at the N_α or N_β atoms of the diazenido complex **[4f″]**, yielded the cationic complexes $\mathbf{[5f'']_{alt}}$ (in a quintet ground state) and $\mathbf{[5f'']_{dis}}$ (in a triplet ground state) respectively (Figure 6.22). The calculated reaction free energies obtained for the formation of $\mathbf{[5f'']_{alt}}$ and $\mathbf{[5f'']_{dis}}$ from the neutral diazenido complex **[4f″]** are considerably exergonic and found to be relatively more exergonic for the distal pathway (Figure 6.23 and Figure 6.24). In addition, we have also calculated the reaction free energy for protonation at the metal center of the diazenido complex **[4f″]**. This reaction is found to be exergonic in nature (-13.8 kcal mol^{-1}) indicating its possibility during the nitrogen reduction process. However, protonation at the sulphur atom of **[4f″]** is computed to be considerably endergonic (22.1 kcal mol^{-1}) which may be attributed to the higher stability of the sulphur lone pair (HOMO-13, E_{LP} = -6.9 eV, Figure 6.25). Furthermore, we have also investigated the activation energy barrier associated with the formation of the cationic species $\mathbf{[5f'']_{alt}}$ and $\mathbf{[5f'']_{dis}}$, from the diazenido complex **[4f″]** by locating the probable TSs. The reaction profile diagram for the conversion of **[4f″]** to $\mathbf{[5f'']_{alt}}$ via the alternating pathway is shown in Figure 6.23. The first step involves the

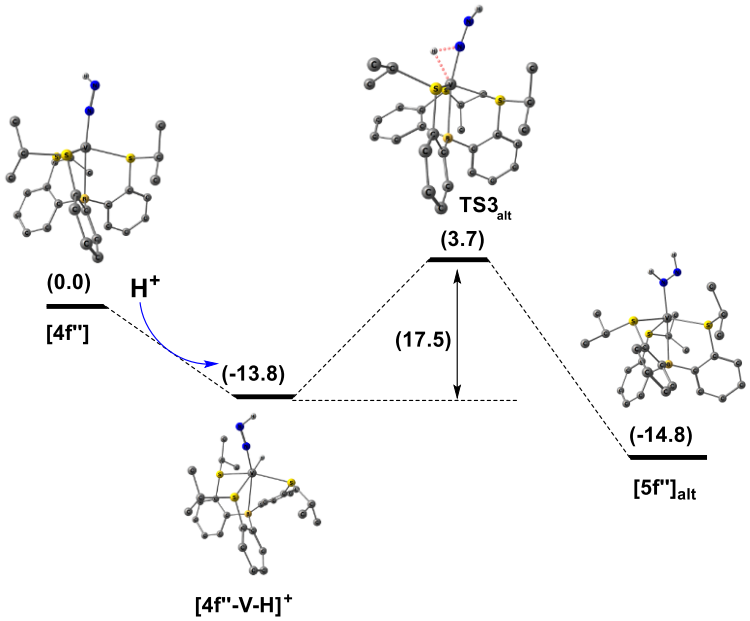

Figure 6.23: Reaction profile diagram for the conversion of **[4f″]** to $\mathbf{[5f'']_{alt}}$ via alternating pathway at M06-L-D3(heptane)/6-311+G* level of theory. Hydrogen atoms of the methyl groups are omitted for clarity. The energy values are in kcal mol^{-1}.

formation of a metal protonated species **[4f″-V-H]**$^{+}$ which lie -13.8 kcal mol^{-1} lower in energy than the starting diazenido complex. Thereafter, the metal protonated species passes through a TS (**TS3$_{alt}$**) with an activation barrier of 17.5 kcal mol^{-1} to generate **[5f″]$_{alt}$**. However, unlike the alternating pathway, two intermediates and two TSs are possible for the transformation of **[4f″]** to **[5f″]$_{dis}$** via the distal pathway (Figure 6.24). The first intermediate, i.e., the metal protonated species **[4f″-V-H]**$^{+}$ is common for both

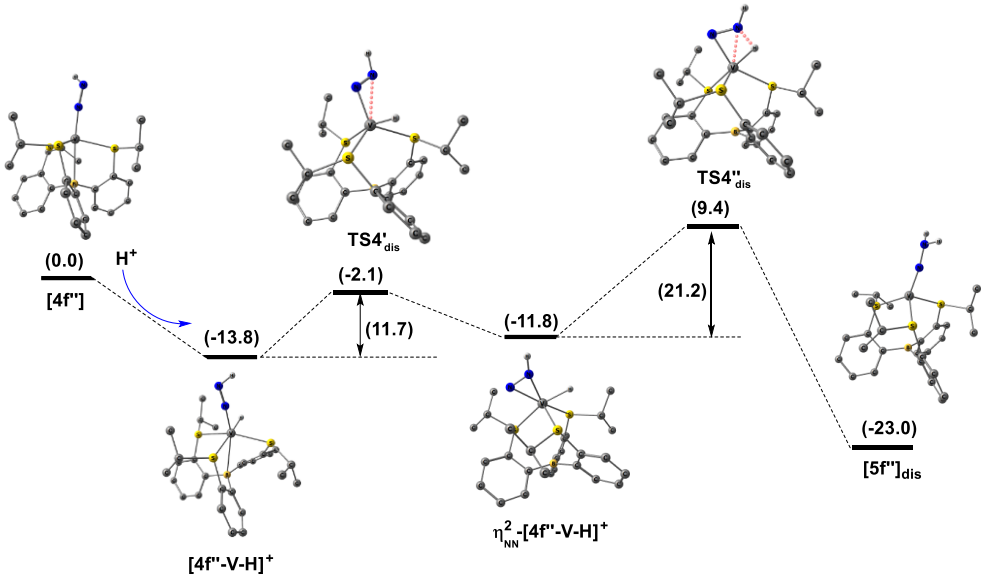

Figure 6.24: Reaction profile diagram for the conversion of **[4f″]** to **[5f″]$_{dis}$** via distal pathway at M06-L-D3(heptane)/6-311+G* level of theory. Hydrogen atoms of the methyl groups are omitted for clarity. The energy values are in kcal mol^{-1}.

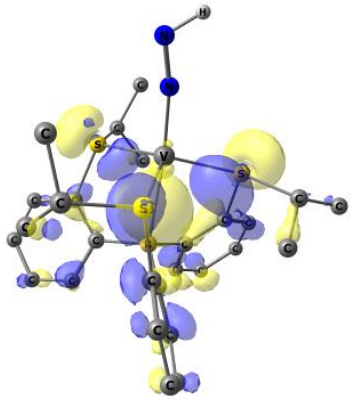

HOMO-13
E_{LP} = -6.9 eV
[4f"]

Figure 6.25: Pictorial representation of the molecular orbital showing the lone pairs situated at the sulphur atoms of the complex **[4f″]**.The hydrogen atoms of the methyl groups are omitted for the sake of clarity.

the pathways that rearranges via a TS (**TS4′$_{dis}$**) with an activation barrier 11.7 kcal mol^{-1} to generate an intermediate in which the metal center is bounded to the two N atoms in η^2 fashion (η^2_{NN}-**[4f″-V-H]**$^+$). Finally, η^2_{NN}-**[4f″-V-H]**$^+$ proceeds through another TS (**TS4″$_{dis}$**) in which the metal bound proton migrates to the β-nitrogen atom to yield **[5f″]$_{dis}$**. The barrier height associated with this transformation is computed to be 21.2 kcal mol^{-1}. Since the transformations **[4f″]→[5f″]$_{dis}$** and **[4f″]→[5f″]$_{alt}$** involves comparable barriers therefore, both pathways may be viable. Further, the possibility of the interconversion of the isomeric species **[5f″]$_{alt}$**, **[6f″]$_{alt}$** and **[7f″]$_{alt}$** to **[5f″]$_{dis}$**, **[6f″]$_{dis}$** and **[7f″]$_{dis}$**, respectively, may be ruled out from thermodynamic (Figure 6.16) and kinetic studies (Figure 6.26). A major difference between the catalysts **[1f″]** and **[1c″]** is

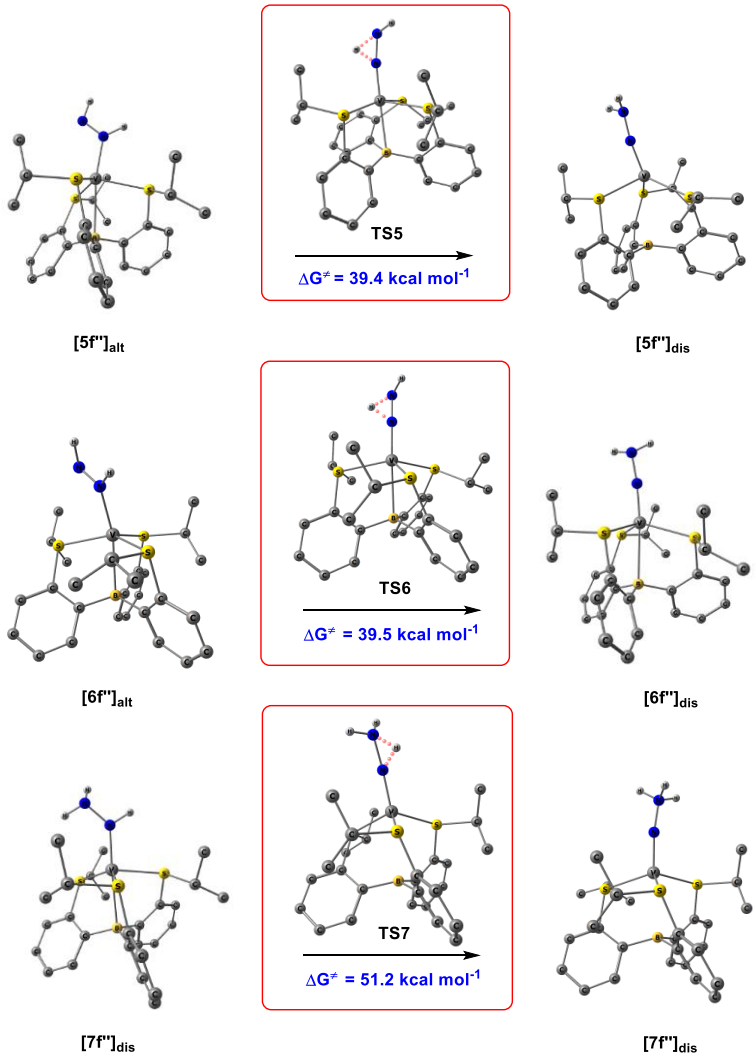

Figure 6.26: Optimized geometries of the TSs involved in the conversion of **[5f″]$_{alt}$**, **[6f″]$_{alt}$** and **[7f″]$_{alt}$** to **[5f″]$_{dis}$**, **[6f″]$_{dis}$** and **[7f″]$_{dis}$** respectively via proton transfer pathway at M06-L-D3(heptane)/6-311+G* level of theory. The hydrogen atoms of the methyl groups are omitted for clarity.

that in the case of **[1f″]**, the equatorial sulfur atom is susceptible to protonation during each phase of protonation. However, protonation at the sulfur atom for each protonation step is computed to be considerably endergonic (11.1 to 27.0 kcal mol^{-1}, Table 6.9), thereby precluding such a possibility. Furthermore, similar to **[1c″]**, the reaction free energies obtained for different steps of the catalytic cycle by employing **[1f″]** were found to be thermodynamically feasible, and also the barrier heights associated with the TSs are low, indicating its potential use as a catalyst for the dinitrogen reduction.

Table 6.9: Calculated (M06-L-D3(heptane)/6-311+G*) reaction free energies (in kcal mol^{-1}) for the protonation at the equatorial sulphur atom of the vanadium complex **[1f″]** at different stages of dinitrogen reduction process. The numbering are given as per Figure 6.22.

Reaction	Equatorial group
[4f″] + H^+	22.1
$[6f'']_{alt}$ + H^+	23.3
$[6f'']_{dis}$ + H^+	16.4
$[8f'']_{alt}$ + H^+	22.5
$[8f'']_{dis}$ + H^+	27.0
$[10f'']_{alt}$ + H^+	11.1
$[10f'']_{dis}$ + H^+	23.2
[12f″] + H^+	21.8

[6.3.5] Dissociation of NH_3 and addition of N_2

The ligand exchange process, which involves the dissociation of NH_3 and addition of N_2, is one of the crucial steps in the dinitrogen reduction process that occurs at the end of the catalytic cycle. Two different mechanisms viz., associative (addition-elimination) and dissociative are possible for such a ligand exchange process. Both experimental [13] and theoretical studies [16, 33] suggested that different routes, viz., anionic, cationic and neutral pathways, are possible for the ligand exchange (N_2/NH_3) reaction (Figure 6.27). Accordingly, all the different pathways were considered while investigating the efficiency of **[1c″]** and **[1f″]** towards the ligand exchange reaction [67]. Furthermore, in a computational study, Reiher and coworkers suggested the formation of a six-coordinated complex for the Schrock's molybdenum catalyst via the associative mechanism [68]. Accordingly, we have also tried to optimize such a complex for our proposed catalysts. However, our catalysts failed to form six coordinated complexes for

the neutral and anionic pathways. The inability to form such complexes may be attributed to the smaller size of the vanadium center to accommodate both the leaving (NH_3) and incoming ligand (N_2) at the metal center simultaneously. Therefore, we expect that our proposed catalysts will follow only the dissociative mechanism for the ligand exchange process. It is clear from Figure 6.27 that for the catalysts **[1c′′]** and **[1f′′]**, the conversion of [V]-NH_3^+ to [V]-N_2^+ via the cationic pathway is thermodynamically unfavorable, which is reflected in the endergonicity associated with this exchange process. However, the other two exchange pathways, viz., anionic and neutral, are thermodynamically viable. Furthermore, for all the pathways, the

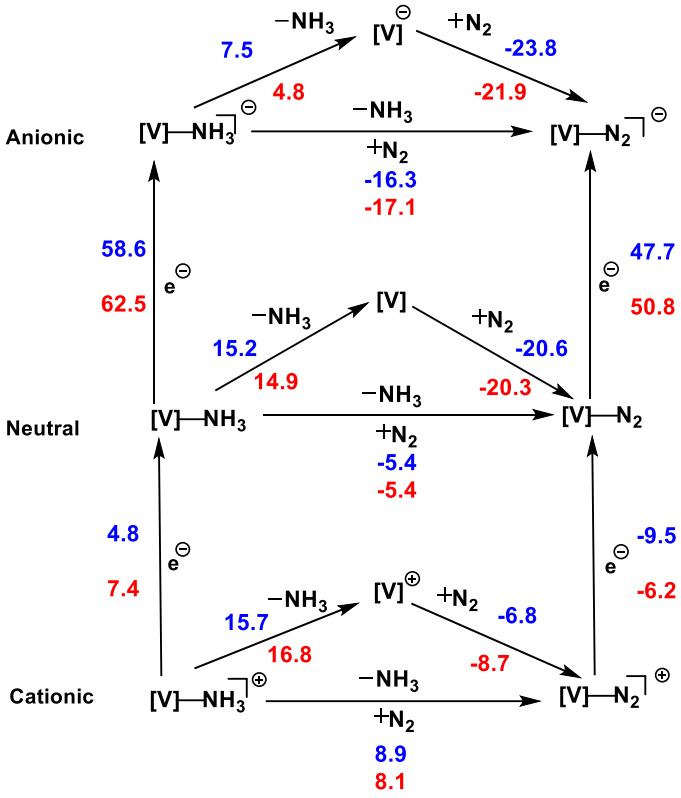

Figure 6.27: Three different possibilities of NH_3/N_2 exchange. The energies are given in kcal mol^{-1} and calculated at M06-L-D3(heptane)/6-311+G*//M06-D3(heptane)/def2-SVP level of theory. The energy values given in *blue* and *red* color corresponds to the catalysts **[1c′′]** and **[1f′′]** respectively.

dissociation of the σ-donor NH_3 is a demanding process as reflected in the endergonic reaction free energies (4.8 to 16.8 kcal mol^{-1}). However, for both the catalysts, the addition of dinitrogen to the vanadium center is computed to be considerably exergonic (-6.8 to -23.8 kcal mol^{-1}). Additionally, reduction (considering $CrCp_2^*$ as the reductant) of [V]-NH_3^+ → [V]-NH_3 is not an energetically demanding process. However, the

subsequent reduction of [V]-NH_3, which results in the formation of an anionic complex [V]-NH_3^-, is calculated to be highly endergonic (as shown in the left hand side of Figure 6.27). Similarly, the reduction process [V]-$N_2^+ \rightarrow$ [V]-N_2 is moderately exergonic (-6.2 to -9.5 kcal mol^{-1}). However, reduction of [V]-N_2 i.e., [V]-$N_2 \rightarrow$ [V]-N_2^- is highly endergonic (47.7 to 50.8 kcal mol^{-1}) in nature. Therefore, unlike the molybdenum catalyst (**I**), which favors both anionic and neutral pathways [16], our calculations suggest that the proposed catalysts **[1c″]** and **[1f″]** should follow only the neutral pathway for the ligand exchange process.

[6.4] Conclusions

Quantum chemical (DFT) calculations have been carried out to study the potential of a series of tripodal vanadium complexes as catalysts in the nitrogen reduction reaction (NRR). All our proposed complexes were found to be capable of dinitrogen functionalization as reflected in the thermodynamic feasibility of several key steps (binding of nitrogen, formation of the diazenido and nitride complex etc.) investigated in this study. For instance, the reaction free energies associated with the formation of N_2 adducts with **[1a′]–[1f′]** and **[1a″]–[1f″]** were found to be substantially exergonic in nature (-18.0 to -23.0 kcal mol^{-1}) thereby indicating their potential in dinitrogen binding. One of the major advantages of these proposed complexes is that they are unlikely to generate hydrazine during the NRR. In addition, we have performed a comprehensive mechanistic study to understand the efficiency of the catalysts **[1c″]** and **[1f″]** by considering all possible pathways viz., alternating and distal pathways, and both thermodynamic and kinetic studies reveal the viability of these two pathways. Our calculations also suggest the possibility of the hybrid distal-to-alternating pathway that may operate during the nitrogen reduction process (as suggested by Peters and coworkers in an earlier report [63]). In addition, interconversion of the isomeric nitrogenous species involved in the alternating (**[5]$_{alt}$**, **[6]$_{alt}$** and **[7]$_{alt}$**) and distal (**[5]$_{dis}$**, **[6]$_{dis}$** and **[7c]$_{dis}$**) pathways is unlikely to occur. Further, there is also scope for protonation at the vanadium center, as indicated by the exergonicity associated with this process. Therefore, this reaction may also compete during the nitrogen reduction process. Furthermore, our calculations demonstrated that the proposed catalysts **[1c″]** and **[1f″]** should follow only the neutral pathway for the ligand exchange process. In addition, both the catalysts are likely to serve as potential candidates for the NRR, which

is evident not only from the calculated highly exergonic reaction free energies of the different steps but also from the moderate barrier heights for the different TSs involved. Therefore, we hope that if one is successful in synthesizing the proposed vanadium complexes, then they may serve as a suitable platform for reducing dinitrogen to ammonia.

[6.5] References

[1] Huheey, J. E., Keiter, E. A., and Keiter, R. L. (1993) *Inorganic Chemistry: Principles of Structure and Reactivity*. Harper Collins College Publishers, New York.

[2] Jennings, J. R. (1991) Catalytic Ammonia Synthesis: Fundamentals and Practice. Springer Science & Business Media.

[3] Schlögl, R. (2008) Ammonia Synthesis. In, Handbook of Heterogeneous Catalysis, of, pages 2501-2575, 3527312412. Wiley-VCH.

[4] Hoffman, B. M., Lukoyanov, D., Yang, Z.-Y., Dean, D. R., and Seefeldt, L. C. Mechanism of Nitrogen Fixation by Nitrogenase: The Next Stage. *Chemical Reviews*, 114(8):4041-4062, 2014.

[5] Kirn, J. and Rees, D. Crystallographic structure and functional implications of the nitrogenase molybdenum–iron protein from Azotobacter vinelandii. *Nature*, 360(6404):553-560, 1992.

[6] Lancaster, K. M., Roemelt, M., Ettenhuber, P., Hu, Y., Ribbe, M. W., Neese, F., Bergmann, U., and DeBeer, S. X-ray Emission Spectroscopy Evidences a Central Carbon in the Nitrogenase Iron-Molybdenum Cofactor. *Science*, 334(6058):974-977, 2011.

[7] Chalkley, M. J., Drover, M. W., and Peters, J. C. Catalytic N_2-to-NH_3 (or-N_2H_4) Conversion by Well-Defined Molecular Coordination Complexes. *Chemical Reviews*, 120(12):5582-5636, 2020.

[8] Scheibel, M. G. and Schneider, S. New Insights into the Biological and Synthetic Fixation of Nitrogen. *Angewandte Chemie International Edition*, 51(19):4529-4531, 2012.

[9] Tanabe, Y. and Nishibayashi, Y. Comprehensive insights into synthetic nitrogen fixation assisted by molecular catalysts under ambient or mild conditions. *Chemical Society Reviews*, 50(8):5201-5242, 2021.

[10] Nishibayashi, Y. Development of catalytic nitrogen fixation using transition metal–dinitrogen complexes under mild reaction conditions. *Dalton Transactions*, 47(33):11290-11297, 2018.

[11] Yandulov, D. V. and Schrock, R. R. Catalytic Reduction of Dinitrogen to Ammonia at a Single Molybdenum Center. *Science*, 301(5629):76-78, 2003.

[12] Schrock, R. R. Catalytic Reduction of Dinitrogen to Ammonia by Molybdenum: Theory Versus Experiment. *Angewandte Chemie International Edition*, 47(30):5512-5522, 2008.

[13] Yandulov, D. V. and Schrock, R. R. Studies Relevant to Catalytic Reduction of Dinitrogen to Ammonia by Molybdenum Triamidoamine Complexes. *Inorganic Chemistry*, 44(4):1103-1117, 2005.

[14] Schrock, R. R. Catalytic Reduction of Dinitrogen to Ammonia at a Single Molybdenum Center. *Accounts of Chemical Research*, 38(12):955-962, 2005.

[15] Studt, F. and Tuczek, F. Energetics and Mechanism of a Room-Temperature Catalytic Process for Ammonia Synthesis (Schrock Cycle): Comparison with Biological Nitrogen Fixation. *Angewandte Chemie International Edition*, 44(35):5639-5642, 2005

[16] Reiher, M., Le Guennic, B., and Kirchner, B. Theoretical Study of Catalytic Dinitrogen Reduction Under Mild Conditions. *Inorganic Chemistry*, 44(26):9640-9642, 2005.

[17] Schenk, S., Le Guennic, B., Kirchner, B., and Reiher, M. First-Principles Investigation of the Schrock Mechanism of Dinitrogen Reduction Employing the full $HIPTN_3N$ ligand. *Inorganic Chemistry*, 47(9):3634-3650, 2008.

[18] Schenk, S., Kirchner, B., and Reiher, M. A Stable Six-Coordinate Intermediate in Ammonia–Dinitrogen Exchange at Schrock's Molybdenum Catalyst. *Chemistry–A European Journal*, 15(20):5073-5082, 2009.

[19] Thimm, W., Gradert, C., Broda, H., Wennmohs, F., Neese, F., and Tuczek, F. Free Reaction Enthalpy Profile of the Schrock Cycle Derived from Density Functional Theory Calculations on the Full $[MoHIPTN_3N]$ Catalyst. *Inorganic Chemistry*, 54(19):9248-9255, 2015.

[20] Arashiba, K., Miyake, Y., and Nishibayashi, Y. A molybdenum complex bearing PNP-type pincer ligands leads to the catalytic reduction of dinitrogen into ammonia. *Nature Chemistry*, 3(2):120-125, 2011.

[21] Eizawa, A., Arashiba, K., Tanaka, H., Kuriyama, S., Matsuo, Y., Nakajima, K., Yoshizawa, K., and Nishibayashi, Y. Remarkable catalytic activity of dinitrogen-bridged dimolybdenum complexes bearing NHC-based PCP-pincer ligands toward nitrogen fixation. *Nature Communications*, 8(1):1-12, 2017.

[22] Anderson, J. S., Rittle, J., and Peters, J. C. Catalytic conversion of nitrogen to ammonia by an iron model complex. *Nature*, 501(7465):84-87, 2013.

[23] Del Castillo, T. J., Thompson, N. B., and Peters, J. C. A Synthetic Single-Site Fe Nitrogenase: High Turnover, Freeze-Quench ^{57}Fe Mössbauer Data, and a Hydride Resting State. *Journal of the American Chemical Society*, 138(16):5341-5350, 2016.

[24] Mankad, N. P., Whited, M. T., and Peters, J. C. Terminal Fe^{I}-N_2 and Fe^{II}···H-C Interactions Supported by Tris (phosphino)silyl Ligands. *Angewandte Chemie International Edition*, 46(30):5768-5771, 2007.

[25] Lee, Y., Mankad, N. P., and Peters, J. C. Triggering N_2 uptake via redox-induced expulsion of coordinated NH_3 and N_2 silylation at trigonal bipyramidal iron. *Nature Chemistry*, 2(7):558-565, 2010.

[26] Stucke, N., Flöser, B. M., Weyrich, T., and Tuczek, F. Nitrogen Fixation Catalyzed by Transition Metal Complexes: Recent Developments. *European Journal of Inorganic Chemistry*, 2018(12):1337-1355, 2018.

[27] Ung, G. and Peters, J. C. Low-Temperature N_2 Binding to Two-Coordinate L_2Fe^0 Enables Reductive Trapping of $L_2FeN_2^-$ and NH_3 Generation. *Angewandte Chemie International Edition*, 54(2):532-535, 2015.

[28] Kuriyama, S. and Nishibayashi, Y. Development of catalytic nitrogen fixation using transition metal complexes not relevant to nitrogenases. *Tetrahedron*, 83:131986, 2021.

[29] Siedschlag, R. B., Bernales, V., Vogiatzis, K. D., Planas, N., Clouston, L. J., Bill, E., Gagliardi, L., and Lu, C. C. Catalytic Silylation of Dinitrogen with a Dicobalt Complex. *Journal of the American Chemical Society*, 137(14):4638-4641, 2015.

[30] Fajardo, J., Jr. and Peters, J. C. Catalytic Nitrogen-to-Ammonia Conversion by Osmium and Ruthenium Complexes. *Journal of the American Chemical Society*, 139(45):16105-16108, 2017.

[31] Kuriyama, S., Arashiba, K., Tanaka, H., Matsuo, Y., Nakajima, K., Yoshizawa, K., and Nishibayashi, Y. Direct transformation of molecular dinitrogen into ammonia

catalyzed by cobalt dinitrogen complexes bearing anionic PNP pincer ligands. *Angewandte Chemie International Edition*, 55(46):14291-14295, 2016.

[32] Smythe, N. C., Schrock, R. R., Müller, P., and Weare, W. W. Synthesis of [(HIPTNCH$_2$CH$_2$)$_3$N]V Compounds (HIPT = 3,5-(2,4,6-*i*-Pr$_3$C$_6$H$_2$)$_2$C$_6$H$_3$) and an Evaluation of Vanadium for the Reduction of Dinitrogen to Ammonia. *Inorganic Chemistry*, 45(23):9197-9205, 2006.

[33] Guha, A. K. and Phukan, A. K. Why Vanadium Complexes Perform Poorly in Comparison to Related Molybdenum Complexes in the Catalytic Reduction of Dinitrogen to Ammonia (Schrock Cycle): A Theoretical Study. *Inorganic Chemistry*, 50(18):8826-8833, 2011.

[34] Sekiguchi, Y., Arashiba, K., Tanaka, H., Eizawa, A., Nakajima, K., Yoshizawa, K., and Nishibayashi, Y. Catalytic Reduction of Molecular Dinitrogen to Ammonia and Hydrazine Using Vanadium Complexes. *Angewandte Chemie International Edition*, 57(29):9064-9068, 2018.

[35] Kokubo, Y., Yamamoto, C., Tsuzuki, K., Nagai, T., Katayama, A., Ohta, T., Ogura, T., Wasada-Tsutsui, Y., Kajita, Y., and Kugimiya, S. Dinitrogen fixation by vanadium complexes with a triamidoamine ligand. *Inorganic Chemistry*, 57(19):11884-11894, 2018.

[36] Kokubo, Y., Wasada-Tsutsui, Y., Yomura, S., Yanagisawa, S., Kubo, M., Kugimiya, S., Kajita, Y., Ozawa, T., and Masuda, H. Syntheses, Characterizations, and Crystal Structures of Dinitrogen-Divanadium Complexes Bearing Triamidoamine Ligands. *European Journal of Inorganic Chemistry*, 2020(15-16):1456-1464, 2020.

[37] Huang, W., Peng, L.-Y., Zhang, J., Liu, C., Song, G., Su, J.-H., Fang, W.-H., Cui, G., and Hu, S. Vanadium-Catalyzed Dinitrogen Reduction to Ammonia via a [V]═NNH$_2$ Intermediate. *Journal of the American Chemical Society*, 145(2):811–821, 2023.

[38] Tanabe, Y. and Nishibayashi, Y. Recent advances in nitrogen fixation upon vanadium complexes. *Coordination Chemistry Reviews*, 381:135-150, 2019.

[39] In our study, we have considered only the bare vanadium complex (i.e., without the attached solvent molecule, THF). Further, in order to reduce the computational cost, the Dipp groups attached to the N atom were replaced with phenyl groups.

[40] Zhao, Y. and Truhlar, D. G. A new local density functional for main-group thermochemistry, transition metal bonding, thermochemical kinetics, and noncovalent interactions. *The Journal of Chemical Physics*, 125(19):194101, 2006.

[41] Francl, M. M., Pietro, W. J., Hehre, W. J., Binkley, J. S., Gordon, M. S., DeFrees, D. J., and Pople, J. A. Self-consistent molecular orbital methods. XXIII. A polarization-type basis set for second-row elements. *The Journal of Chemical Physics*, 77(7):3654-3665, 1982.

[42] Rassolov, V. A., Pople, J. A., Ratner, M. A., and Windus, T. L. 6-31G* basis set for atoms K through Zn. *The Journal of Chemical Physics*, 109(4):1223-1229, 1998

[43] Rassolov, V. A., Ratner, M. A., Pople, J. A., Redfern, P. C., and Curtiss, L. A. 6-31G* basis set for third-row atoms. *Journal of Computational Chemistry*, 22(9):976-984, 2001.

[44] Gusev, D. G. Assessing the Accuracy of M06-L Organometallic Thermochemistry. *Organometallics*, 32(15):4239-4243, 2013.

[45] Yamout, L. S., Ataya, M., Hasanayn, F., Holland, P. L., Miller, A. J., and Goldman, A. S. Understanding Terminal versus Bridging End-on N_2 Coordination in Transition Metal Complexes. *Journal of the American Chemical Society*, 143(26):9744-9757, 2021.

[46] Averkiev, B. B. and Truhlar, D. G. Free energy of reaction by density functional theory: oxidative addition of ammonia by an iridium complex with PCP pincer ligands. *Catalysis Science & Technology*, 1(8):1526-1529, 2011.

[47] Chamkin, A. A., and Serkova, E. S. DFT, DLPNO-CCSD(T), and NEVPT2 benchmark study of the reaction between ferrocenium and trimethylphosphine. *Journal of Computational Chemistry*, 41(28):2388-2397, 2020.

[48] Gu, N. X., Oyala, P. H., and Peters, J. C. Hydrazine Formation via Coupling of a Nickel(III)–NH_2 Radical. *Angewandte Chemie International Edition*, 60(8):4009-4013, 2021.

[49] Gu, N. X., Oyala, P. H., and Peters, J. C. H_2 Evolution From a Thiolate-Bound Ni(III) Hydride. *Journal of the American Chemical Society*, 142(17):7827-7835, 2020.

[50] Raju, R. K., Bengali, A. A., and Brothers, E. N. A unified set of experimental organometallic data used to evaluate modern theoretical methods. *Dalton Transactions*, 45(35):13766-13778, 2016.

[51] Graziano, B. J., Vollmer, M. V., and Lu, C. C. Cooperative Bond Activation and Facile Intramolecular Aryl Transfer of Nickel–Aluminum Pincer-type Complexes. *Angewandte Chemie International Edition*, 60(27):15087-15094, 2021.

[52] Cammarota, R. C., Xie, J., Burgess, S. A., Vollmer, M. V., Vogiatzis, K. D., Ye, J., Linehan, J. C., Appel, A. M., Hoffmann, C., and Wang, X. Thermodynamic and kinetic studies of H_2 and N_2 binding to bimetallic nickel-group 13 complexes and neutron structure of a Ni(η_2-H_2) adduct. *Chemical Science*, 10(29):7029-7042, 2019.

[53] Cossi, M., Scalmani, G., Rega, N., and Barone, V. New developments in the polarizable continuum model for quantum mechanical and classical calculations on molecules in solution. *The Journal of Chemical Physics*, 117(1):43-54, 2002.

[54] Grimme, S., Antony, J., Ehrlich, S., and Krieg, H. A consistent and accurate ab initio parametrization of density functional dispersion correction (DFT-D) for the 94 elements H-Pu. *The Journal of Chemical Physics*, 132(15):154104, 2010.

[55] Glendening, E. D., Reed, A. E., Carpenter,J. E., and Weinhold, F. NBO Program 3.1, W. T. Madison, 1988.

[56] Frisch, M. J., Trucks, G. W., Schlegel, H. B., Scuseria, G. E., Robb, M. A., Cheeseman, J. R., Montgomery, J. A., Jr., Vreven, T., Kudin, K. N., Burant, J. C., Millam, J. M., Iyengar, S. S., Tomasi, J., Barone, V., Mennucci, B., Cossi, M., Scalmani, G., Rega, N., Petersson, G. A., Nakatsuji, H., Hada, M., Ehara, M., Toyota, K., Fukuda, R., Hasegawa, J., Ishida, M., Nakajima, T., Honda, Y., Kitao, O., Nakai, H., Klene, M., Li, X., Knox, J. E., Hratchian, H. P., Cross, J. B., Bakken, V., Adamo, C., Jaramillo, J., Gomperts, R., Stratmann, R. E., Yazyev, O., Austin, A. J., Cammi, R., Pomelli, C., Ochterski, J. W., Ayala, P. Y., Morokuma, K., Voth, G. A., Salvador, P. J., Dannenberg, J., Zakrzewski, V. G., Dapprich, S., Daniels, A. D., Strain, M. C., Farkas, O., Malick, D. K., Rabuck, A. D., Raghavachari, K., Foresman, J. B., Ortiz, J. V., Cui, Q., Baboul, A. G., Clifford, S., Cioslowski, J., Stefanov, B. B., Liu, G., Liashenko, A., Piskorz, P., Komaromi, I., Martin, R. L., Fox, D. J., Keith, T., Al- Laham, M. A., Peng, C. Y., Nanayakkara, A., Challacombe, M., Gill, P. M. W., Johnson, B., Chen, W., Wong, M. W., Gonzalez, C., and Pople, J. A. *Gaussian 03*, *Revision D.02*; Gaussian, Inc., Pittsburgh, PA, 2003.

[57] Benedek, Z., Papp, M., Oláh, J., and Szilvási, T. Exploring Hydrogen Evolution Accompanying Nitrogen Reduction on Biomimetic Nitrogenase Analogs: Can Fe–NxHy

Intermediates Be Active Under Turnover Conditions?. *Inorganic Chemistry*, 58(12):7969-7977, 2019.

[58] Junge, J., Engesser, T. A., and Tuczek, F. N_2 Reduction versus H_2 Evolution in a Molybdenum-or Tungsten-Based Small-Molecule Model System of Nitrogenase. *Chemistry–A European Journal*, 29(13):e202202629, 2023.

[59] Gogoi, U., Guha, A. K., and Phukan, A. K. Tracing the Route to Ammonia: A Theoretical Study on the Possible Pathways for Dinitrogen Reduction with Tripodal Iron Complexes. *Chemistry–A European Journal*, 19(33):11077-11089, 2013.

[60] Barney, B. M., Lukoyanov, D., Yang, T. C., Dean, D. R., Hoffman, B. M., and Seefeldt, L. C. A methyldiazene ($HN=N-CH_3$)-derived species bound to the nitrogenase active-site FeMo cofactor: Implications for mechanism. *Proceedings of the National Academy of Sciences*, 103(46):17113-17118, 2006.

[61] Thompson, N. B., Green, M. T., and Peters, J. C. Nitrogen Fixation via a Terminal Fe(IV) Nitride. *Journal of the American Chemical Society*, 139(43):15312-15315, 2017.

[62] G, Jafari, M., Fehn, D., Reinholdt, A., Hernández-Prieto, C., Patel, P., Gau, M. R., Carroll, P. J., Krzystek, J., Liu, C., and Ozarowski, A. Tale of Three Molecular Nitrides: Mononuclear Vanadium (V) and (IV) Nitrides As Well As a Mixed-Valence Trivanadium Nitride Having a V_3N_4 Double-Diamond Core. *Journal of the American Chemical Society*, 144(23):10201-10219.

[63] Rittle, J., and Peters, J. C. An Fe-N_2 Complex that Generates Hydrazine and Ammonia via $Fe=NNH_2$: Demonstrating a Hybrid Distal-to-Alternating Pathway for N_2 Reduction. *Journal of the American Chemical Society*, 138(12):4243-4248.

[64] Kuriyama, S., Arashiba, K., Nakajima, K., Matsuo, Y., Tanaka, H., Ishii, K., Yoshizawa, K., and Nishibayashi, Y. Catalytic transformation of dinitrogen into ammonia and hydrazine by iron-dinitrogen complexes bearing pincer ligand. *Nature Communications*, 7(1):12181, 2016.

[65] Fajardo Jr, J., and Peters, J. C. Tripodal $P_3XFe–N_2$ Complexes (X= B, Al, Ga): Effect of the Apical Atom on Bonding, Electronic Structure, and Catalytic N_2-to-NH_3 Conversion. *Inorganic Chemistry*, 60(2):1220-1227, 2021.

[66] Creutz, S. E., and Peters, J. C. Catalytic Reduction of N_2 to NH_3 by an $Fe–N_2$ Complex Featuring a C-atom Anchor. *Journal of the American Chemical Society*, 136(3):1105-1115, 2014.

[67] Despite several attempts, we could not optimize the parent reduced species **[V]**$^-$ at M06-L-D3(heptane)/6-311+G*. However, the same reduced species can be optimized at M06-D3(heptane)/def2-SVP level of theory. Accordingly, the complete ligand exchange process was investigated by using the M06-L-D3(heptane)/6-311+G*//M06-D3(heptane)/def2-SVP level of theory.

[68] Schenk, S., Kirchner, B., and Reiher, M. A Stable Six-Coordinate Intermediate in Ammonia–Dinitrogen Exchange at Schrock's Molybdenum Catalyst. *Chemistry–A European Journal*, 15(20):5073-5082, 2009.